(13)

Performance of Uncooled 1.3 μm FP and DFB Lasers in Hybrid Fiber-Coax (HFC) Networks

by

Sofia Gebru

Submitted to the Department of Electrical Engineering and Computer Science in partial fulfillment of the requirements for the degree of

Master of Engineerirng in Electrical Engineering and Computer Science

at the

MASSACHUSETTS INSTITUTE OF TECHNOLOGY

February 7, 1997

© Sofia Gebru, 1997. All rights reserved.

The author hereby grants to MIT permission to reproduce and distribute publicly paper and electronic copies of this thesis in whole or in part, and to grant others the right to do so.

Author _____
Department of Electrical Engineering and Computer Science
February 7, 1997

Certified by _____
Professor Cardinal Warde
Department of Electrical Engineering and Computer Science
Thesis Supervisor

Accepted by _____
Frederic .R. Morganthaler
Chairman, Department Committee on Graduate Theses

MASSACHUSETTS INSTITUTE OF TECHNOLOGY

MAR 21 1997

LIBRARIES

Performance of Uncooled 1.3 μ m FP and DFB Lasers in Hybrid Fiber-Coax (HFC) Networks

by

Sofia Gebru

Submitted to the
Department of Electrical Engineering and Computer Science

February 7, 1997

In partial fulfillment of the requirements for the degree of Masters
of Engineering in Electrical Engineering and Computer Science

ABSTRACT

The purpose of this thesis was to investigate the performance of uncooled 1.3 μ m lasers in the temperature range of -40° C to 85° C when used for QPSK transmission in HFC networks. Both Fabry-Perot (FP) and distributed feedback (DFB) lasers were studied. Two different optical packages, one with an optical isolator and one without, were investigated. The variations of laser electro-optical characteristics and their effects on QPSK transmission were measured as the temperature was varied. Both FP and DFB lasers have a wide range of optical modulation index (OMI) for which error free QPSK transmission was observed. DFB lasers are more sensitive to reflections from the fiber than FP lasers. When an optical isolator was used, the error free transmission range of the lasers was improved by at least 15 dB. The signal to noise ratio (SNR) for the system changed by as much as 2 dB over the temperature range from -40° C to 25° C, and changed by as much as 9.7 dB over the temperature range from 25° C to 85° .

Thesis Supervisor: Cardinal Warde
Title: Professor, MIT - EECS

Table of Contents

Acknowledgment

I would like to thank V. Swaminathan and Nan Froberg at Lucent Technologies for their technical guidance throughout the project, for patiently and thoroughly going through the draft of this thesis, and for giving me very insightful comments. I would also like to thank Ron Sorensen and S. Lee for helping me with the experiments. I would like to thank J. P. Moffat and Amit Singh for their helpful discussions in the course of the experiments.

I would like to thank Jay Fahey for giving me the opportunity to do my thesis at Lucent Technologies and Professor Cardinal Warde for agreeing to be my supervisor on campus.

I would also like to thank my friend Fekade Aytaged for reading my drafts and providing me with insightful comments.

List of Figures

List of Tables

List of Abbreviations

AM-VSB - Amplitude Modulation - Vestigial Side Band

BER - Bit Error Rate

DEMUX - Demultiplexer

DFB - Distributed Feedback

FP - Fabry Perot

FSK - Frequency Shift Keying

HFC - Hybrid Fiber Coax

IF -Intermediate Frequency

IIN - Interferometric Intensity Noise

MQW - Multiple Quantum Wells

NLD - Non-Linear Distortion

OMI - Optical Modulating Index per Channel

QPSK - Quadrature Phase Shift Keying

RF - Radio Frequency

RIN - Relative Intensity Noise

RMS - Root Mean Square

SCMA - Sub-Carrier Multiple Access Network

SNR - Signal to Noise Ratio

1. Introduction

The hybrid fiber-coax (HFC) network is one of the network options that service providers are considering to offer broadband services such as broadcast video, interactive TV, digital video, data, and telephony via fiber from the headend or central office to a fiber node and then from the fiber node to subscriber homes via coaxial cables.

The serving area of an HFC network can vary from 200-2000 homes per fiber node. The HFC architecture consists of a fiber going from the headend to a fiber node near subscribers' homes from which coaxial cables carry the broadband services to the homes. Each fiber node can be split into quadrants for which services are transported over coaxial cables. In one of the commercially deployed HFC networks, the quadrant serves 120 subscribers such that each fiber node serves about 480 homes [1].

A typical HFC frequency plan to transmit all broadband services goes from 5 - 750 MHz. The frequency spectrum from 54 - 750 MHz (downstream) is used by the headend to transmit the broadband services while the frequency spectrum from 5 - 40 MHz (upstream) is used by the subscribers to send a signal to the central office such as data and telephony. The frequency spectrum from 54 - 550 MHz is used to transmit broadcast analog video, the frequency spectrum from 550 - 700 MHz is used to transmit digital video, and the frequency spectrum from 700 - 750 MHz is used to transmit data and telephony. The 40 - 54 MHz bandwidth is taken up by the filter that separates the downstream and upstream signals [1].

Currently, cooled and isolated distributed feedback (DFB) lasers are used as transmitters for the fiber optic portion of HFC for both the downstream and upstream paths. However, incorporating the cooling and isolation mechanisms significantly increases the size and cost of the lasers. Also lasers used for narrow band services such as voice in both the downstream and upstream directions are used in pairs to provide redundancy. This increases the number of narrowband transmitters and thus the initial cost of installation. Thus, research has been done to investigate the use of unisolated and uncooled DFB and FP lasers for narrowband applications especially for the return path in HFC networks. Since the upstream traffic will initially consist of data and telephony services that do not place as stringent a requirement on the laser as video services, uncooled and unisolated lasers may work as well for the return path [1].

Since the return path lasers in HFC networks are deployed in a fiber node outside the headend or central office, it is necessary to study the performance of uncooled and unisolated FP and DFB lasers when the ambient temperature of the system changes significantly. For the upstream services quadrature phase shift keying (QPSK) modulation is generally employed and it has already been demonstrated that uncooled and unisolated FP [2] and DFB lasers are capable of transmitting error free QPSK signals. The performance of uncooled and unisolated DFB[3] lasers has also been studied when the ambient temperature changes significantly. It is expected that the performance of the lasers will degrade when the temperature is increased. It is the goal of this experiment to characterize the behavior of uncooled and unisolated FP lasers when the ambient temperature changes so that the performance of FP lasers can be fully determined for the upstream path. The FP lasers are of special interest because they are cheaper than the DFB lasers that are currently used as transmitters for the upstream path for data and telephony services.

2. Theory

In order to understand the issues involved in analyzing the performance of FP and DFB lasers, it is necessary to review the basic theory underlying the HFC network and specifically the technology used to transmit QPSK signals in the upstream path. The lasers that are used, the QPSK modulation technique, and various mechanisms that degrade the performance of the lasers as well as the system in general will be reviewed.

2. 1 Lasers

One of the lasers being considered for use in the HFC upstream path is an uncooled Fabry-Perot laser. A Fabry-Perot laser consists of an active (light emitting) semiconductor material sandwiched between two mirrors. The basic structure looks as follows.

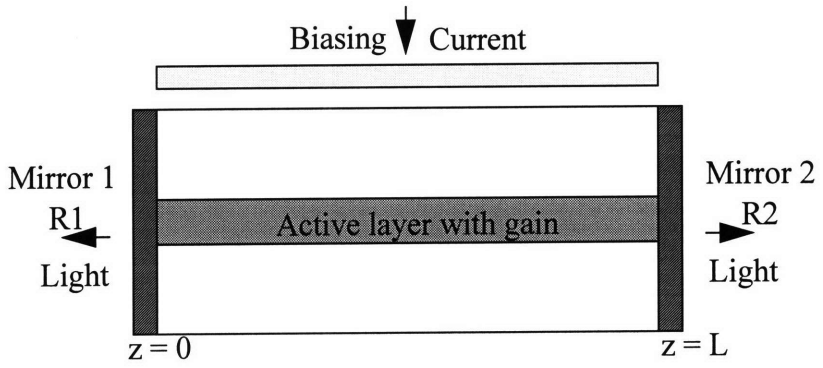

Figure 1: Fabry-Perot Laser

The current is used to bias the laser so that population inversion is achieved and there can be stimulated emission of coherent light. The two mirrors are used as feedback such

that the light that is emitted is passed through the active material several times and is amplified. The light output of a Fabry-Perot laser versus the injected current is given as $Pout(I) = \eta_d\left(\frac{h\nu}{2e}\right)(I - I_{th})$. I_{th} is the threshold current above which lasing takes place, η_d is the external quantum efficiency defined as the photon escaping rate to the photon generation rate, ν is the optical frequency, h is Planck's constant, and e is the electronic charge [4].

The Fabry-Perot laser is a multi-longitudinal mode laser where there are different frequencies that can lase. The different frequencies that can lase are given by $2kL = 2\pi m$ where m is the mode of the Fabry-Perot cavity, k is the wave number, L is the length of the Fabry-Perot cavity [4].

A DFB laser, unlike an FP laser, is a single longitudinal mode laser. In a DFB laser, the feedback mechanism for lasing is accomplished by a grating that varies periodically along the laser cavity. Thus, the refractive index along the grating also varies periodically. This causes some of the launched waves into the cavity to get reflected back from the grating. Coherent coupling between a forward and a backward propagating wave will occur for wavelengths which satisfy the Bragg condition. Lasing occurs only at wavelengths which satisfy the condition $\Lambda = \frac{m\lambda_m}{2}$ where Λ is the grating period, λ_m is the wavelength of the light inside the gain medium, and m is the order of the Bragg diffraction. Thus, by choosing an appropriate grating period Λ , wavelength selectivity is achieved. The structure of a DFB laser is shown below [5].

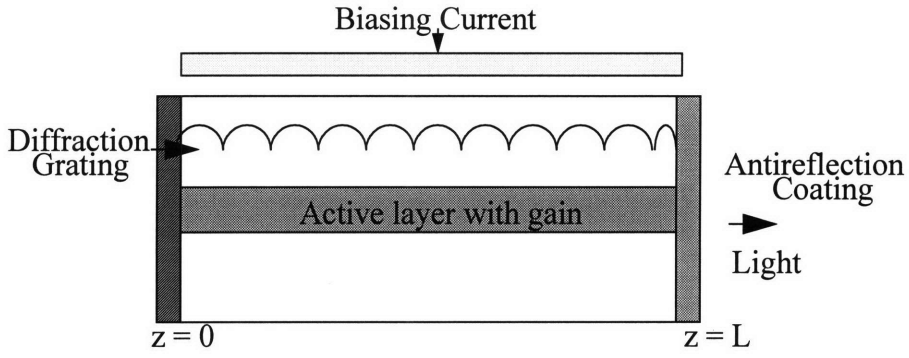

Figure 2: DFB Laser

Similar to the light output characteristics of an FP laser, the light output of a DFB laser versus the biasing or threshold current is given as $Pout(I) = \eta_d\left(\frac{h\nu}{2e}\right)(I - I_{th})$.

Several reasons make the DFB lasers more attractive than the FP lasers for use in optical communication systems. First of all, DFB lasers emit in a single longitudinal mode. This makes them more attractive than FP lasers because fiber dispersion together with mode partition noise causes intersymbol interference for QPSK modulation using multi-longitudinal mode FP lasers. Fiber dispersion causes different pulses to propagate at different speeds within the fiber and arrive at the output of the fiber overlapped. Mode partition noise, which is caused by shift in the frequency of the gain spectrum of the laser while it is being modulated, along with fiber dispersion causes intersymbol interference when the pulses propagate within the fiber [6]. As will be discussed later, the DFB laser has also a very linear light output versus current which lowers distortions due to interference between many analog carriers modulating the same laser. On the other hand, DFB lasers

are more sensitive to reflections than FP lasers which can degrade the performance of the DFB lasers when they are used without optical isolators [5].

The performance of both the FP and DFB lasers degrades as temperature increases. The threshold current increases with temperature exponentially according to $I_{th}(T) = I_o \exp\left(\frac{T}{T_o}\right)$ where I_o is the current measured at temperature T_o. T_o is the characteristic temperature used to express the temperature sensitivity of the lasers and varies from 50° to 70° Kelvin [7].

There are different reasons why the threshold current increases with increasing temperature. Depending on the specific structure of the laser, part of the injected current is lost as leakage current and not available for injection into the active layer. Also, some of the injected carriers recombine non-radiatively. Both the leakage current and non-radiative current increase with temperature causing the threshold current to increase and the external quantum efficiency η_d to decrease [7].

2.2 Optical Isolator

Currently, the DFB lasers used in the HFC upstream and downstream paths employ an optical isolator. An optical isolator is a device used in laser packages and it prevents reflected light from splices and other discontinuities from entering into the laser. Reflections into the laser increase the laser intensity fluctuations which show up as noise and degrade laser performance.

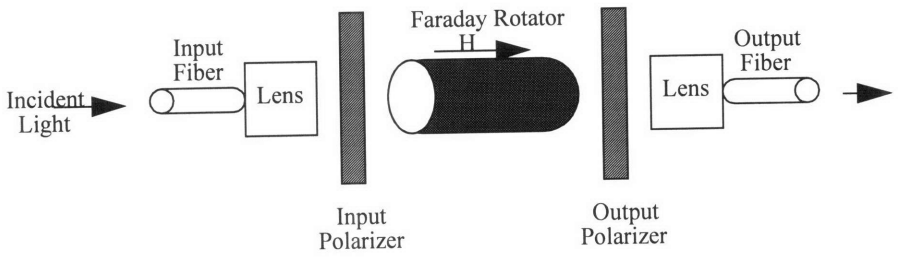

Figure 3: Optical Isolator

A basic optical isolator consists of an input polarizer followed by a Faraday rotator followed by another polarizer (analyzer). The first polarizer passes the component of the incident light that has a polarization parallel to it. The Faraday rotator changes the polarization of the incident wave by a magnitude that is linearly proportional to the magnetic field applied and the length of interaction of the light with the rotator. The change of polarization as a function of the magnetic field is given by $\alpha = \zeta HL$ where α is the rotation in degrees, ζ is Verdet's constant, H is the magnetic field, and L is the length of interaction of the light with the rotator [8].

When an incident light goes through an optical isolator, it will experience a change in the polarization of magnitude α degrees when first going through the Faraday rotator. The light then goes through the analyzer which has the same orientation as the angle of rotation α. When the reflected light comes back, it goes through the analyzer again and only the component of the reflected light that has a polarization α passes through. When the light goes through the Faraday rotator, it experiences another rotation of magnitude α but in a different direction than that the incident field experienced. Thus, when the light

reaches the input polarizer, its polarization will be at an angle 2α with respect to the input polarizer. Therefore, the reflected light will be highly attenuated depending on the magnitude of α when passing through the first polarizer. For maximum attenuation, α can be set to 45 degrees so that when the reflected light reaches the first polarizer, the polarization of the light is orthogonal to the orientation of the first polarizer [8].

2.3 QPSK Modulation

The modulation scheme currently employed for transmitting data and telephony in the downstream path is quadrature phase shift keying (QPSK). For many existing coaxial cable networks the modulation used for return path traffic is frequency shift keying (FSK). The modulation scheme for transmitting broadcast analog video (NTSC TV) in the downstream path is amplitude modulated vestigial sideband (AM-VSB) while the one for transmitting digital video is quadrature amplitude modulation (64 QAM) [1].

In HFC networks, QPSK modulation is considered for return path in order to increase bandwidth efficiency for transmitting data and telephony signals. The basic mechanism for generating a QPSK modulated signal is shown below.

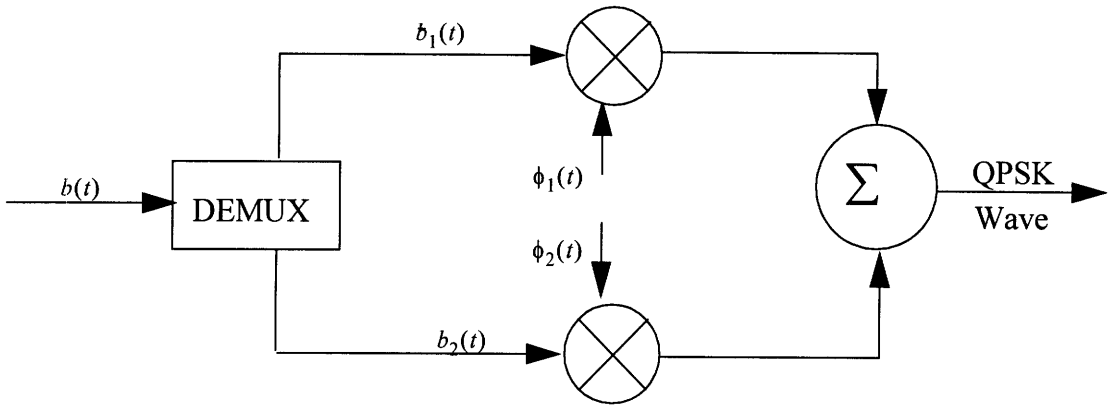

Figure 4: QPSK Modulator

The input binary wave is divided into an odd and even numbered bit sequence by a demultiplexer. The two binary waves, denoted by $b_1(t)$ and $b_2(t)$ then modulate a pair of quadrature waves denoted by $\phi_1(t)$ and $\phi_2(t)$ where $\phi_1(t) = \sqrt{\frac{2}{T}}\cos(2\pi f_c t)$ and $\phi_2(t) = \sqrt{\frac{2}{T}}\sin(2\pi f_c t)$. f_c is the carrier frequency given by $\frac{n_c}{T}$, where T is the duration of the symbol, and n_c is a fixed integer. The two modulated signals are added and we get the QPSK modulated wave [9].

The QPSK modulated wave can be represented by

$$s_i(t) = \sqrt{\frac{2E}{T}}\cos\left[(2i-1)\frac{\pi}{4}\right]\cos(2\pi f_c t) - \sqrt{\frac{2E}{T}}\sin\left[(2i-1)\frac{\pi}{4}\right]\sin(2\pi f_c t) \qquad \text{for } 0 \le t \le T$$

where $i = 1, 2, 3, 4$. The symbol 1 is represented by a voltage level $\sqrt{E}$ and the symbol 0 is represented by a voltage level $\sqrt{E}$ [9].

At the receiver, the signal will become contaminated by noise which is modeled as a white Gaussian noise $w(t)$. The received signal will be $x(t) = s_i(t) + w(t)$ where

$i = 1, 2, 3, 4$ and the given equation holds for $0 \le t \le T$. The QPSK receiver (demodulator) is shown below [9].

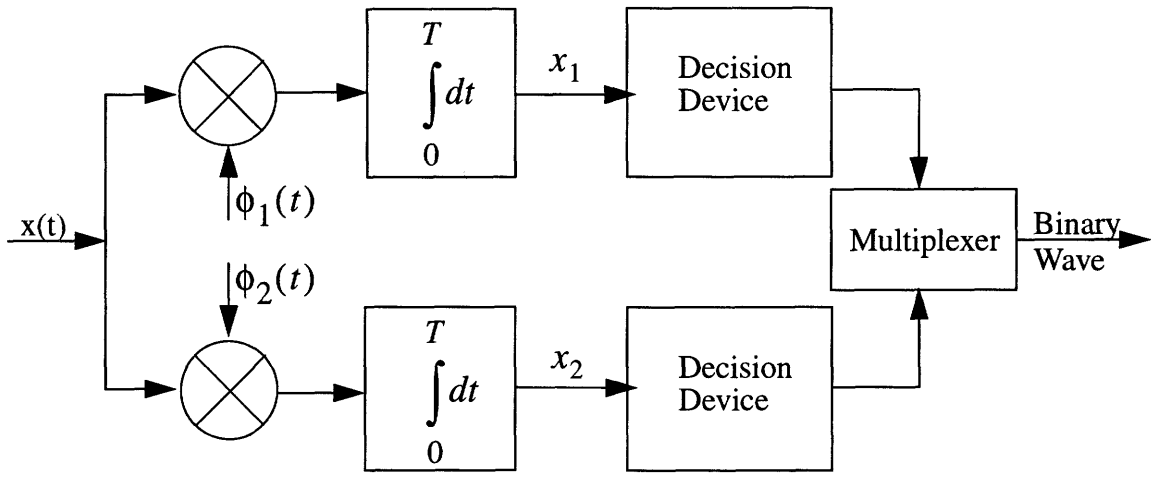

Figure 5: QPSK Demodulator

The received signal $x(t)$ is multiplied by the two local oscillators $\phi_1(t)$ and $\phi_2(t)$. The generated signal then goes through an integrator. The signal x_1 is given by [9]

$$x_1 = \int_0^T x(t)\phi_1(t)dt = \sqrt{E}\cos\left[(2i-1)\frac{\pi}{4}\right] + w_1$$ and the signal x_2 is given by

$$x_2 = \int_0^T x(t)\phi_2(t)dt = -\sqrt{E}\cos\left[(2i-1)\frac{\pi}{4}\right] + w_2 \quad .$$

Then, x_1 and x_2 will be compared against zero volts. If either one is greater than zero volts, a decision in favor of symbol 1 will be made. If either one is smaller than zero volts, a decision in favor of symbol 0 will be made. The two binary sequences that were selected

are then combined with the multiplexer and the initial transmitted binary signal is recovered [9].

At the decision making device, an erroneous decision can be made so that the bits that were transmitted will not be received. The probability of making an erroneous decision is the probability of making a decision to choose symbol 1 when the transmitted symbol is 0 or the probability of making a decision to choose symbol 0 when the transmitted symbol is 1. This is approximately given by $P_e \approx erfc\left(\sqrt{\frac{E_b}{N_o}}\right)$ where erfc is the complementary error function given by $erfc(x) = \frac{2}{\pi}\int_x^\infty \exp(-z^2)dz$. E_b is the transmitted energy per bit, which is half the transmitted energy per symbol E . $\frac{N_o}{2}$ is the variance of the white Gaussian noise, $w(t)$. Since there are two bits per symbol, the bit error rate for a QPSK modulated wave is half the symbol error rate and is given by $BER = \frac{P_e}{2} \approx \frac{erfc}{2}\left(\sqrt{\frac{E_b}{N_o}}\right)$ [9].

2.4 Subcarrier Multiaccess Network (SCMA)

The basic mechanism by which the QPSK signals are transmitted in the HFC network is by using multiple channel subcarrier multiplexing. In this mechanism, the digital data being transmitted is used to QPSK modulate an RF carrier which is then used to modulate an optical signal. The subcarrier refers to the RF carrier and the main carrier is the optical signal [10].

For semiconductor laser sources with linear light vs. current curves, the total output power when the QPSK signal modulates the laser is given by

$P_i(t) = P_{bi}(t)\{1 + m_i a_i \cos(2\pi f_i t + \phi_i)\}$ where P_{bi} is the optical output power, m_i is the optical modulation index, and a_i is the normalized amplitude of the RF drive which is either 1 or 0. The modulation index m_i is defined as the ratio of the amplitude of the RF carrier to the optical power output, $m_i = \frac{P_i^{max} - P_{bi}}{P_{bi}}$ [10].

At the head-end or central office, an optical receiver converts the optical signal into an electrical signal. The electrical signal is amplified and goes through an RF bandpass filter to select the channel of interest. The frequency of the desired channel is down converted to IF using a local oscillator at the demodulator [10].

2.5 Types Of Noise Affecting QPSK Transmission

There are several sources of noise that degrade the signal to noise ratio in a fiber optic QPSK transmission. These are the shot noise of the optical receiver, the thermal noise of the optical receiver, the laser intensity noise, and the laser clipping induced noise. Note that in our experiments, we consider only the noise sources in the optical link of the return path. In the return path of an HFC network, there are other noise contributions such as the modem noise, noise in the coaxial plant, and other noise in the RF portion of the distribution. The noise contributions in the optical path will be discussed next.

2.5.1 Shot Noise

The shot noise arises in the optical receiver because of the random nature of the photons that impinge on the photodetector and give rise to the flow of electrons. Because of

the randomness of the arriving photon stream, the generated current at the output of the photodetector is also a random distribution characterized by a mean and a variance. The variance of the current from its average value is the shot noise of the receiver. It is given by

$$\sigma_{shot}^2 = \langle [i_{0,1}(t) - \bar{I}_{0,1}]^2 \rangle = 2e\bar{I}_{0,1}\Delta f = 2eR\bar{P}_{0,1}\Delta f$$

where $i_{0,1}(t)$ is the instantaneous current corresponding to bits 0 and 1, $\bar{I}_{0,1}$ is the average current out of the photodetector, e is the electronic charge, R is the responsivity of the photodiode defined as ratio of the current generated to the photon incident, Δf is the effective noise bandwidth of the receiver and $\bar{P}_{0,1}$ is the average power incident at the receiver [11].

2.5.2 Receiver Noise

The receiver noise is caused by the thermal noise of the load resistor that changes the current from the photodetector into voltage and by the front-end amplifier that amplifies the voltage to usable levels. The thermal noise is the noise caused by the random motion of the electrons inside the resistor when the temperature is above absolute zero. The electron fluctuations inside the resistor cause a current fluctuation. The variance of the current fluctuation σ_{th}^2 around a zero mean thermal current is given by $\sigma_{th}^2 = \langle i_{th}^2 \rangle = \frac{4kT\Delta f}{R_L}$ where k is Boltzmann's constant, T is the absolute temperature, R_L is the load resistor, and Δf is the bandwidth of the receiver [11]. The receiver noise is given by $\sigma_{rc}^2 = \langle i_{rc}^2 \rangle = \frac{4kT\Delta fNF}{R_L}$ where NF is the noise figure of the ampli-

fier. The receiver noise is usually given as a noise current per square root hertz and is of the order of 8-12 $\frac{pA}{\sqrt{Hz}}$ [12].

2.5.3 Laser RIN and Fiber IIN

The laser intensity noise at the receiver is caused by the superposition of the stimulated or coherent emission of the light on the spontaneous emission of the light. Since the spontaneous emission of the light is random, the fluctuations in the intensity of the spontaneous emission cause a fluctuation in the intensity and phase of the power output of the coherent light which shows up as noise. These intensity and phase fluctuations are characterized by the laser relative intensity noise (RIN) which is the power spectral density of the normalized output power fluctuations. The RIN is given as the autocorrelation of the normalized fluctuation of the output power as:

$$RIN(f) = \int_{-\infty}^{\infty}\left(\int_{-\infty}^{\infty} \delta P(t)\delta P(t+\tau)dt\right)e^{i2\pi ft}d\tau$$

where $\delta P(t) = \frac{(P(t)-\bar{P})}{\bar{P}}$. $\bar{P}$ is the average output power of the laser diode, $P(t)$ is the instantaneous output power, and $\delta P(t)$ is the normalized output power fluctuation of the laser. The RIN goes as P^{-3} at low output powers (i.e when the bias current is near the threshold current) and as P^{-1} at high output powers. The RIN is also given as $RIN \propto \left(\frac{I_b}{I_{th}} - 1\right)^{-3}$ for the bias current I_b greater than the threshold current I_{th} [13].

The laser noise power σ_{RIN}^2 is given by $\sigma_{RIN}^2 = (RP_b)^2 RIN\Delta f$ where R is the responsivity of the receiver, P_b is the average received optical power, and Δf is the noise bandwidth of the receiver [14].

It is known that the fiber spool in the transmission path from the headend (or central office) to the fiber node increases the level of the laser relative intensity noise (RIN) through interferometric intensity noise (IIN) from the fiber. The IIN is caused by reflections from the fiber either through Rayleigh backscattering in the fiber or through reflections from inhomogeneities in the fiber which convert laser phase noise into laser intensity noise. The IIN contribution to the RIN of the laser depends on the laser linewidth and fiber attenuation. It is given by $IIN(f) = \frac{4R_f^2}{\sqrt{2\pi}B_{\frac{1}{2}}}$ where R_f if the fiber reflectivity and $B_{\frac{1}{2}}$ is the laser half linewidth [15]. In the presence of the fiber, the contribution of IIN should be added to RIN in estimating the laser intensity noise. In subsequent sections, the RIN will be used to refer to the laser intrinsic RIN and IIN unless otherwise noted.

2.5.4 Laser Clipping Noise

When the RF drive level is very high, clipping of the laser occurs and gives rise to noise. Clipping occurs when the modulating current goes below the threshold current. The modulated optical power cannot be negative so the optical power goes to zero when the modulating power goes below zero. Clipping of the laser places an upper limit on the number of subcarriers that can be used and the maximum RF power at which they can operate.

The clipping noise power or the total nonlinear distortion caused by the clipping of the subcarriers is analyzed by modeling the sum of the power of each modulated carrier as a function of time as a Gaussian random process with mean power P_b and variance $\sigma_p^2 = \frac{NP_b^2 m^2}{2}$. N is the number of modulated subcarriers and m is the modulation index of each of the subcarriers [16]. The total nonlinear distortion will then be given by the probability of the power $P(t)$, which falls below zero and causes the laser power to go to zero. The nonlinear distortion along with some modification is given by $NLD = \frac{1}{4N}\sqrt{\frac{2}{\pi}}\frac{(RP_b)^2\mu^5}{(1+6\mu^2)}\exp\left(-\frac{1}{2\mu^2}\right)$ [17] where R is the responsivity of the photodiode and μ is the root mean square (rms) modulation index given by $\mu = m\sqrt{\frac{N}{2}}$.

2.6 Signal to Noise Ratio For HFC

The multiple subcarrier multiplexed system (HFC) performance can be analyzed using signal to noise ratio (SNR) measurements where the different noise mechanisms that degrade the system performance will be included. The signal to noise ratio is defined as the root-mean-square (rms) carrier power to the total rms noise power. Thus, for the HFC network, the SNR is given by $SNR = \frac{Carrier}{NLD + \sigma_{RIN}^2 + \sigma_{rc}^2 + \sigma_{shot}^2}$. The carrier power is given by $Carrier = \frac{(mRP_o)^2}{2}$ where m is the modulation index, R is the responsivity of the receiver, and P_o is the optical output power. Since the current out of the photodiode is given by $I_o = RP_o$, and the modulation index of each carrier can be written as $m^2 = \frac{2\mu^2}{N}$, the signal power can also be written as $Carrier = \frac{\mu^2}{N}I_o^2$ where N is the number of modulated subcarriers. Thus, the overall simplified expression for the signal to noise ratio is given as:

$$SNR = \frac{\mu^2 I_o^2}{N\left[NLD + \sigma_{RIN}^2 + \sigma_{rc}^2 + \sigma_{shot}^2\right]}$$

Further substitution of the noise elements and simplification gives the SNR [17]as,

$$SNR = \frac{\mu^2 I_o^2}{N\Delta f\left[\frac{NLD}{N\Delta f} + I_o^2 RIN(f) + i_{rc}^2 + 2eI_o\right]}$$

where Δf is the effective bandwidth of the receiver, and i_{rc} is the receiver noise current per square root hertz.

In order to analyze the performance of the lasers used to transmit the QPSK signals in the HFC network, the bit error rate of the QPSK transmission system is also measured. In terms of the signal to noise ratio (SNR), the bit error rate (BER) for the QPSK signal is given approximately as $BER \approx \frac{1}{2} erfc\left(\sqrt{\frac{SNR}{2}}\right)$ assuming that the noise in the transmission channel is a white Gaussian noise [18].

2.7 Intermodulation Distortions

There are other factors that degrade the performance of the HFC optical path but do not degrade the signal to noise ratio. Intermodulation distortions in a multiple subcarrier multiplexed system such as HFC occurs because of the nonlinearity of the light source. When a single light source is modulated by various RF subcarriers, the various subcarriers are mixed within the laser cavity. This introduces new intermodulation products at differ-

ent powers that appear at new frequencies that depend on the placing of the main subcarrier frequencies. If these intermodulation products appear within the bandwidth of the channel under consideration they degrade the performance of the system. If one octave of bandwidth is used for all the channels, second order intermodulation distortions will not be present. The intermodulation distortions in the HFC optical path are measured by measuring the signal to intermodulation tone ratio (SIM). Even if the SNR is large, if the SIM is not as large, there will be error in the transmitted signal due to the interfering tone. Thus, for error free performance, it is desirable to have the signal to intermodulation tone ratio at least as large as the required SNR [17].

3. Approach

Various experiments were performed in order to analyze the performance of uncooled and unisolated and uncooled and isolated FP and DFB lasers when they transmitted QPSK signals in the HFC network at room temperature. These experiments consisted of measuring the BER of QPSK signals as a function of SNR and OMI of the laser. The measurement of BER versus OMI is used to determine the range of RF drive levels to achieve reliable (error free) QPSK transmission. Similarly, measuring the BER versus the SNR gives the required SNR for reliable transmission.

The SNR of the system versus the OMI of the lasers was also measured. This is because it is desirable to operate the lasers at the OMI where the maximum SNR is achieved since when the QPSK signal is sent through the HFC network, there are other noise contributions besides the ones affecting the optical transmission path that are discussed in Section 2. These noise contributions typically arise from the coaxial cable that is used as the final transmission medium to the home, the RF modulator at the customers' premises, and the RF demodulator at the headend.

The effect of the fiber on QPSK transmission was also investigated. It is known that the fiber increases the RIN of the laser because of IIN. The fiber effect also manifested as spurious reflections producing interfering tones at random frequencies within the transmission bandwidth. The spurious noise cannot be effectively measured just by the measurement of RIN and IIN. Therefore, the effect of the spurious noise on the BER performance of the unisolated FP and DFB lasers was investigated by comparing the BER performance with and without the fiber. In the experiment without the fiber, the 4.7 dB of

loss of the fiber was maintained by increasing the insertion loss between the laser and the receiver via a jumper cable with rotary connectors. When spurious noise was present, adding an optical isolator in the transmission path greatly minimized its effect and improved BER performance. This led us to study the performance of uncooled and isolated FP and DFB lasers also.

Once the performance of the uncooled and unisolated and uncooled and isolated FP and DFB lasers at room temperature was analyzed, the above experiments were repeated as a function of temperature. That is the BER and SNR of the system were measured at various temperatures. The RIN of the lasers was also measured when the temperature was varied to see how the lasers' noise characteristic changed with temperature.

4. Experimental Setup

The experimental setup used to perform the various measurements is shown below.

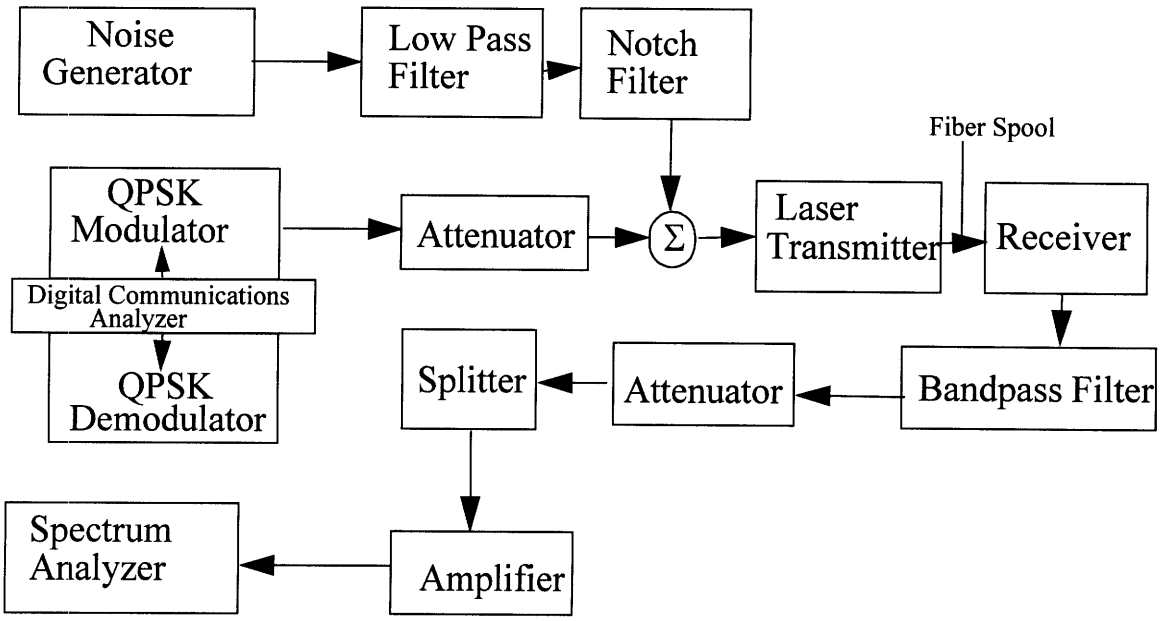

Figure 6: Experimental Setup

The digital communication analyzer sends a 1.54 Mb/s pseudo-random bit sequence to the QPSK modulator. The resulting QPSK wave goes through an attenuator and gets coupled with a noise generator. The noise generator in the figure above is a wideband noise generator and its signal is passed through a low pass filter and a notch filter. The low pass filter has a passband from 5-40 MHz. The notch filter enabled placing the 750 KHz wide QPSK channel at 14 MHz in the 5-40 MHz passband. The noise generator simulated the modulation of the laser with forty QPSK channels. The attenuator in the QPSK modulator

is used to adjust the power of the QPSK signal driving the laser. There is also an attenuator that is part of the noise generator to adjust the power of the simulated QPSK channels.

The combined payload of the noise and the QPSK signal is used to modulate an unisolated or isolated and uncooled FP or DFB laser. The output of the laser transmitter then goes through 12 km of single mode fiber with 4.7 dB of attenuation to simulate a typical HFC system.

The optical signal is converted into an electrical signal by a 5-200 MHz return path receiver. The RF signal is then sent through a bandpass filter and the filtered signal is sent through an attenuator. The two signals are split two ways after going through the attenuator. The attenuator is used to keep the input signal level to the QPSK demodulator in the range from 5 dBmV to -12 dBmV. In all the experiments, the input level to the QPSK demodulator was maintained at approximately 2 dBmV. The other output of the two way splitter is sent through an amplifier and the output is monitored using a spectrum analyzer. The amplifier is used so that the measured noise of the system on the spectrum analyzer is at least 10 dB above the noise floor of the spectrum analyzer in order to make accurate measurements of the noise of the system.

The demodulated bit stream is sent to the digital communication analyzer where the instrument directly compares the received bits to the generated bits. The BER is the ratio of the bits that are received in error to the number of bits that are generated in a two minute interval.

Once the room temperature measurements have been made, the laser transmitter is kept in a temperature oven in order to look at the temperature variations of the system.

5. Experimental Procedure

The way the BER of the system is measured versus the OMI of the laser is as follows. First, the attenuator that is attached to the QPSK modulator is used to change the QPSK drive level. The noise level is also attenuated by the same amount as the QPSK signal to keep the equivalent RF power/channel the same. The digital communication analyzer gives the BER of the system for the different QPSK and noise drive levels.

The OMI at each transmitter level is measured by using a circuit that uses a calibrated pin photodiode. The output of the laser transmitter is connected directly to the pin photodiode. A voltmeter is used to measure the dc voltage corresponding to the photocurrent, I_{dc}. The output of the pin photodiode is connected to the spectrum analyzer and the power P_{rf} of the RF signal that is modulating the laser is measured. The modulation index m is then given by $m = \frac{\sqrt{2\frac{P_{rf}}{R_L}}}{I_{dc}}$. Since $m = \frac{I_{rf}}{I_{dc}}$ where I_{rf} is the RF current given by $P_{rf} = \frac{I_{rf}^2 R_L}{2}$ and R_L is the impedance of the system and is 75 Ω. Since the RF signal power is measured in dBm on the spectrum analyzer, the modulation index m is actually calculated as

$$m = \frac{\sqrt{\frac{2000\left(10^{\frac{P_{rf}}{10}}\right)}{75}}}{I_{dc}}$$

where P_{rf} is the measured RF power in dBm and I_{dc} is in mA.

The SNR is measured by first measuring the level of the QPSK signal using the RF spectrum analyzer. The resolution bandwidth of the spectrum analyzer is set to 1 MHz, the

video bandwidth of the spectrum analyzer is set to 30 KHz, and the video average function of the spectrum analyzer is set to 100. The resolution bandwidth is set to 1 MHz so that it is closer to the signal bandwidth to make an accurate measurement of the QPSK carrier power. The SNR is calculated in the QPSK symbol bandwidth. For the data rate of 1.54 Mb/s, the symbol rate is $\frac{1.54}{2}$ Mb/s for QPSK modulation since there are 2 bits/symbol. Thus, the measured SNR is given by $SNR = Signal - \left(Noise + 10\log\left(\frac{1.55\exp(6)}{2}\right)\right)$ which when simplified gives $SNR = Signal - (Noise + 58.8)$.

By changing the drive level of the QPSK signal and the noise, and by measuring the different OMI levels, the OMI versus the SNR was obtained. At each OMI, the BER was also measured to obtain BER versus SNR.

The RIN and IIN of the laser is found by connecting the output of the laser transmitter to the spectrum analyzer and using the RIN measuring feature of the spectrum analyzer. The spectrum analyzer uses the incident power to calculate the shot noise and thermal noise for the optical receiver in the spectrum analyzer. It then subtracts these terms from the total noise of the system to give the RIN of the laser. That is *RIN = Measured Noise - Thermal Noise - Shot Noise*.

Once the above experiments were performed at room temperature, the experiments were repeated by putting the laser transmitter into a temperature oven. Once the optimum RF drive level or OMI was found at room temperature, it was kept the same but the temperature was varied in intervals of 10° C to 15° C from -40° C to 85° C. The SNR, BER, and RIN were measured after allowing the laser to reach thermal equilibrium at each temperature.

6. Room Temperature Measurements

Four unisolated and uncooled lasers, two FP and two DFB lasers were tested. Two isolated FP lasers and one isolated DFB laser were also tested. All lasers tested had multiple quantum wells (MQW) and were made of InGaAsP. The lasers were biased using a bias-tee circuit shown below. The dc current to the laser was adjusted such that the optical output power at the fiber pigtail was around 980μ Watts.

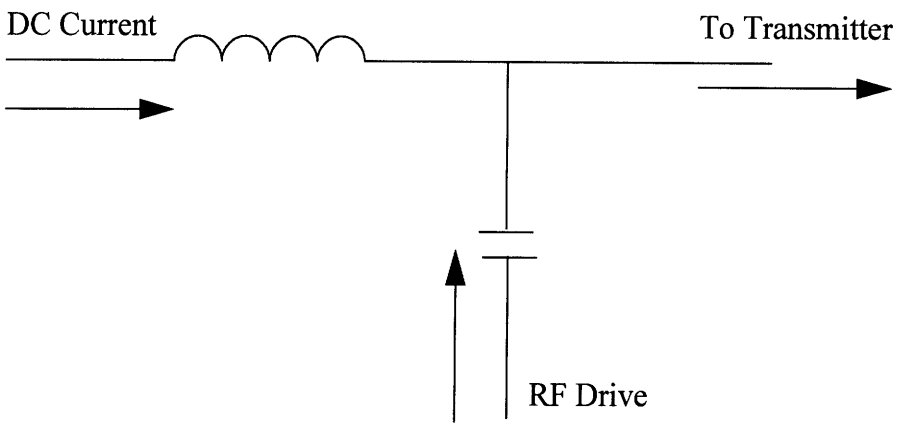

Figure 7: Bias-Tee Circuit

The parameters OMI, SNR, and BER were measured for each of the lasers tested and plots of SNR versus BER, OMI versus BER, and OMI versus SNR were obtained for the unisolated and isolated lasers. The effects of the fiber spool on the BER and SNR performance of the lasers was also investigated.

6.1 Performance of Unisolated FP and DFB Lasers Without Fiber Spool

The performance of the lasers without fiber is examined first so that the effect of spurious reflections introduced by the fiber can be clearly assessed. As was discussed in Section 3, the effect of the fiber spool was investigated by comparing the BER performance of the FP and DFB lasers with and without the fiber. In the experiment without the fiber which will be discussed in this section, the 4.7 dB of loss of the fiber was maintained by increasing the insertion loss between the laser and the receiver via a jumper cable with rotary connectors. The BER performance of the lasers is compared against the theoretically expected BER performance for QPSK modulated data. The theoretical BER expected for a QPSK modulated data and the performance of the modulator and demodulator back-to-back will be discussed next.

6.1.1 Theoretical BER and Modem Noise

For reliable transmission of data a BER less than 10^{-8} is required while for telephony a BER less than 10^{-9} is required [19]. In the presence of only white Gaussian noise, a minimum SNR of 15 dB is required for a BER on the order of 10^{-8} or less and a minimum SNR of 16 dB is required for a BER of 10^{-9} or less [19]. Figure 8 shows the theoretically expected BER for QPSK modulated data in the presence of only white Gaussian noise [18]. In the experiments described here, zero error in a 2-minute counting interval is arbitrarily taken to be as BER of 10^{-9} as shown on the plots.

The back-to-back performance of the modulator and demodulator without the laser transmitter is also shown on Figure 8. It can be seen from the plot that the back-to-back

performance of the QPSK modem used deviates very little from the theoretically expected performance indicating that the impairment in BER caused by modem noise is not significant. For this reason, the modem noise is not considered in the discussions below.

6.1.2 BER versus SNR

For both the unisolated and uncooled FP and DFB lasers tested BER less than 10^{-9} was observed for SNR values greater than or equal to 17 dB for all the lasers [Table 1]. As can be seen from Figure 9a (FP lasers) and Figure 9b (DFB lasers), both the FP and DFB lasers show similar BER performance. It can also be seen from the plots that the BER performance of both types of lasers is close to the theoretically expected BER performance for a QPSK modulated data. When no error was measured for a 2-minute interval, the BER was arbitrarily set at 10^{-9} .

6.1.3 BER versus OMI

Figure 10a and Figure 10b show the BER versus OMI for unisolated FP and DFB lasers, respectively. As can be seen on the plots for these lasers, error free transmission was observed for OMI in the range from 0.1%-10% for three of the four lasers tested. However, DFB Laser D started clipping at an OMI of 7.3%. As the OMI increases beyond 10% for the other lasers, the BER increases due to laser clipping at high modulation index levels. The maximum OMI values for the different lasers are given in Table 1. When the OMI is low, the system performance is limited by the thermal and shot noise of the optical receiver and the BER starts to increase if the OMI goes below 0.1% for all the lasers

tested. The error free transmission range within the upper and lower limits set by the clipping of the laser and by the thermal and shot noise of the optical receiver is referred to as the error free dynamic range of the lasers in this work.

Table 1 shows the maximum and minimum OMI and the corresponding SNR for which error free transmission was observed for the FP and DFB lasers. Note again that in this experiment, when no BER was measured in a 2-minute interval, the BER was arbitrarily set to 10^{-9}. The subscripts Mx and Mn next to the RF drive level, OMI, and SNR, indicate the maximum and minimum RF drive level and OMI for which error free transmission was observed and the corresponding SNR. There is a ± 1 dB error in the SNR and RF drive level measurements. Also Laser A and laser C are from the same vendor whereas laser B and laser D are from different suppliers.

Table 1: Performance of Lasers at the Maximum and Minimum OMI Without Fiber

Laser (Type)	η_d	RF $Drive_{Mx}$	OMI_{Mx}	SNR_{Mx}	RF $Drive_{Mn}$	OMI_{Mn}	SNR_{Mn}	Dynamic Range
	$\frac{\mu Watts}{mA}$	dBmV	%	dB	dBmV	%	dB	dB
Laser A (FP)	100	37.46	11.3	20.7	-7.54	0.074	18	47
Laser B (FP)		41.46	12.8	17.3	-2.54	0.18	18.5	45
Laser C (DFB)	120	33.46	11.9	22.1	-12.54	0.065	17.8	49
Laser D (DFB)		25.46	7.3	21.9	-17.54	0.067	16	44

It can be seen from the table that the DFB lasers need less RF drive to reach the same OMI as the FP lasers which is due to the fact that the DFB lasers have a higher external quantum efficiency, η_d, than the FP lasers.

In these experiments, the DFB lasers behaved similar to the FP lasers in as far as the clipping noise limited the BER performance. This is in contrast to the results of Woodward et al.[3] who observed that DFB lasers did not show any clipping induced impairment on BER even at an rms OMI (μ) of 100%. In this experiment the highest μ to achieve BER less than 10^{-9} is 53% for the DFB lasers. This is calculated by $\mu = \sqrt{\frac{N}{2}} OMI$ where N, the number of carriers, is 40. In the present experiment, a noise source was used to simulate the number of QPSK carriers in the 5-40 MHz band, whereas in the previous experiment, unmodulated carriers from a matrix box in the 55-400 MHz band were used. Either the frequency plan or the channel loading or both could play a role on BER. Further experiments are needed to understand this discrepancy.

6.1.4 SNR Versus OMI

The SNR versus the OMI per channel for each of the unisolated FP and DFB lasers without fiber was measured. It can be seen from Figure 12a for the FP lasers and Figure 12b for the DFB lasers that the SNR becomes a maximum at a certain OMI but then decreases when the OMI becomes very high or very low. The shape of the plots shown are consistent with simulations done using the equation for the SNR where $SNR = \frac{\mu^2 I_o^2}{N\Delta f\left[\frac{NLD}{N\Delta f} + I_o^2 RIN(f) + i_{th}^2 + 2eI_o\right]}$. All the terms in the expression for the SNR

are defined in section 2.6.

At high OMI levels, the lasers are clipped and the clipping induced noise degrades the SNR. When the OMI is low, the system performance is limited by the thermal and shot noise of the optical receiver. Thus, at low OMI levels, the SNR is low.

As can be seen on Figure 12a and Figure 12b, laser A and laser B which are unisolated FP lasers had a maximum SNR of 53.5 dB and 44.5 dB, respectively while lasers C and D which are unisolated DFB lasers had a maximum SNR of 52.2 dB and 45.9 dB respectively. This maximum SNR occurred at an OMI of 5.0% and 5.8%, respectively for the FP lasers while the DFB lasers attained their maximum SNR at an OMI of 5.0% and 3.0%, respectively. The difference in the OMI and maximum SNR values for these lasers can be attributed to their particular laser structure and their linearity about which information was not provided by the suppliers. It is however worth noting that the SNR of the two FP lasers and the two DFB lasers from different suppliers can vary over a wide range. For example, the FP and DFB lasers shown in Table 2 have SNR values differing by 7-9 dB. This means that when multiple sources are used to procure the lasers for upstream applications, careful evaluations need to be performed to qualify different suppliers. The drive level and OMI at which the maximum SNR occurs along with the maximum SNR for these lasers are summarized in Table 2.

Table 2: Maximum SNR of Unisolated FP and DFB Lasers Without Fiber

Supplier	Laser	η_d	RF Drive	OMI	Maximum SNR
		$\frac{\mu Watts}{mA}$	dBmV	%	dB
X	Laser A (FP)	100	29.46	5.2	53.5
Y	Laser B (FP)		32.46	5.8	44.5
X	Laser C (DFB)	120	23.46	5.0	52.2
Z	Laser D (DFB)		17.46	3.0	45.9

6.2 Performance of Unisolated FP and DFB Lasers With Fiber Spool

When the OMI is low, the system performance is limited by the thermal and shot noise of the receiver as seen in Section 6.1 for the case without fiber. However, when the fiber is present in the optical transmission path, spurious reflections that were generated from the fiber degraded the BER performance of the laser even for OMI values much above the minimum values required to overcome the laser shot, thermal, and RIN noises. Monitoring the spectral band of the QPSK channel in a spectrum analyzer, we observed spurious spikes which had enough RF power to give a signal-to-interfering-noise ratio to cause BER. The spurious reflections from the fiber were not dependent on the supplier of the fiber because a similar behavior was obtained with different fiber spools with the same loss. A plot of how the spurious noise appears on the spectrum analyzer is attached in Appendix A.

6.2.1 BER versus SNR

The BER versus SNR performance for the lasers with fiber is shown in Figure 13a for FP lasers and Figure 13b for DFB lasers. It can be seen that for SNR values greater than or equal to 17 dB, two types of BER performance were observed. For the same SNR, both error free as well as high BER is observed. For example, at a SNR of 27 dB, BER on the order of 10^{-8} is observed. The error free as well as the high BER correspond to regions of high and low OMI values, respectively. As the laser OMI is increased and commensurately SNR increases, error free BER performance is observed only at sufficiently high SNR values. This can be seen in Figure 13a and Figure 13b, where there are high BER on the order of 10^{-8} even when the SNR is as high as 39 dB for the DFB lasers. This is in contrast to the case without fiber where no error was seen at such a high SNR.

With further increase in the OMI as the laser approaches the clipping limit, the SNR decreases and the BER performance follows the theoretically expected behavior. In the clipping limit, the BER performance of the lasers versus the SNR with the fiber was similar to the BER performance of the laser without the fiber for both the FP and DFB lasers. Both the FP and DFB lasers show similar BER performance. This can be seen on Figure 13a (FP lasers) and Figure 13b (DFB lasers).

6.2.2 BER versus OMI

When the OMI was near the clipping limit, the BER performance of the lasers when the fiber was present in the transmission path was similar to the performance of the lasers

when the fiber was not present. The maximum OMI beyond which clipping occurred was similar for the lasers with and without the fiber.

When the OMI is decreased below approximately 1%, BER as high as 10^{-8} were measured due to the spurious reflections from the fiber. The error free dynamic range for both the FP and DFB lasers was decreased when the fiber was used. In contrast, as can be seen from Figure 14a and Figure 14b, when the fiber is removed, OMI can be decreased by almost an order of magnitude to as low as approximately 0.1% and still error free performance can be achieved.

In terms of the transmitter drive level, the error free dynamic range was reduced by 21 dB and by 16 dB, respectively, for lasers A and B in the presence of fiber compared to the case when no fiber was present [Figure 15a]. Since the noise floor of laser B is higher than the noise floor of laser A, the fact that the dynamic range improvement of laser B's is not as high as laser A's is consistent. For the DFB lasers, as can be seen from Figure 15b, the error free dynamic range was reduced because of the fiber by 25 dB and by 21 dB for lasers C and D, respectively.

Table 3 shows the maximum and minimum OMI and the corresponding SNR for which error free transmission was observed for the FP and DFB lasers with the fiber spool in the transmission path. Note again that in this experiment, when no BER was measured in a 2-minute interval, the BER was arbitrarily set to 10^{-9}. Again, the subscripts Mx and Mn next to the RF drive level, OMI, and SNR, indicate the maximum and minimum RF drive level and OMI for which error free transmission was observed and the corresponding SNR.

Table 3: Performance of Unisolated Lasers at the Maximum and Minimum OMI With Fiber

Laser (Type)	η_d	RF $Drive_{Mx}$	OMI_{Mx}	SNR_{Mx}	RF $Drive_{Mn}$	OMI_{Mn}	SNR_{Mn}	Dynamic Range
	$\frac{\mu Watts}{mA}$	dBmV	%	dB	dBmV	%	dB	dB
Laser A (FP)	100	38.46	11.0	19.2	16.46	1.2	40.3	26
Laser B (FP)		40.46	11.8	18	17.46	1.0	30.7	28
Laser C (DFB)	120	34.46	12.4	20.3	12.46	1.2	40	24
Laser D (DFB)		25.46	7.3	21.8	7.46	1.0	37.7	23

6.2.3 SNR versus OMI

The OMI versus SNR performance of the lasers with or without the fiber was similar. This can be seen on Figure 16a and Figure 16b. The maximum SNR for all the lasers and the OMI and RF drive level at which the maximum SNR occurred is summarized in Table 4.

Table 4: Maximum SNR of Unisolated FP and DFB Lasers With Fiber

Supplier	Laser	η_d	RF Drive	OMI	Maximum SNR
		$\frac{\mu Watts}{mA}$	dBmV	%	dB
X	Laser A	100	30.46	5.5	51.4
Y	Laser B		31.46	5.1	42.6

Table 4: Maximum SNR of Unisolated FP and DFB Lasers With Fiber

Supplier	Laser	η_d	RF Drive	OMI	Maximum SNR
X	Laser C	120	23.46	3.6	48.5
Z	Laser D		17.46	3.0	41.6

However, the maximum SNR when the fiber was present decreased. This was due to the increase in the noise in the presence of the fiber which will be discussed next.

6.2.4 Effect of Fiber Spool on the Noise, RIN, and SNR

When the fiber spool was used, the maximum SNR decreased by at least 3.5 dB for the DFB lasers and by at least 2 dB for the FP lasers. This can be seen by comparing the SNR values in Table 2 and Table 4. The decrease in the SNR was entirely due to the increase in the noise level at the OMI where the maximum SNR occurs when the fiber is used. The increase in the noise level was about 4 dB for the DFB lasers and about 2 dB for the FP lasers at the OMI where the maximum SNR occurred. Also, an overall increase in the noise level of at least 2 dB for the FP lasers and at least 2.5 dB for the DFB lasers was observed in the error free window of OMI. In the regions of OMI where clipping noise and the thermal and shot noise dominated, the noise level was about the same for both experiments with or without the fiber.

In the error free OMI window, the increase in noise is predominantly due to the increase in RIN. This is shown in Table 5 which compares RIN measured with and without fiber. About 4 dB increase in RIN is observed for the FP lasers when the fiber was

present. When the fiber is removed, the IIN contribution to the noise of the system is removed as well.

Even though the total RIN is lower for DFB lasers than FP lasers, DFB lasers are more sensitive to reflections from the fiber and other splices [3]. This explains why the noise level for the DFB lasers improved more with the removal of the fiber than the noise level of the FP lasers did.

Table 5: RIN With and Without Fiber

Laser	RIN plus IIN	RIN
	(dB/Hz)	(dB/Hz)
FP Laser A	-142.35	-145.37
FP Laser B	-132.74	-136.69

6.2.5 Summary of Results for Unisolated FP and DFB Lasers

Both FP and DFB uncooled and unisolated lasers produce error-free QPSK transmission (BER less or equal 10^{-9}) for the upstream path. What is noteworthy is that FP lasers behaved as good as DFB lasers for data and telephony services. Since DFB lasers are more sensitive to reflections, in the absence of an optical isolator, FP lasers are preferred over DFBs. There is also a wide range of OMI from 1% to 10% for the FP lasers for which the error is less than 10^{-9}. Thus, the unisolated and uncooled FP lasers are suitable for transmission of both data and telephony. Since unisolated and uncooled DFB lasers can be as much as $400 more expensive than the unisolated and uncooled FP lasers, using FP lasers

in the upstream path for data and telephony services is a preferred decision both in terms of cost and performance.

For both the FP and DFB lasers, it was seen that the fiber reduced the maximum SNR that can be achieved and also reduced the error free dynamic range. The fiber degraded the maximum SNR of the DFB lasers more than the FP lasers. However, in any real system the fiber is always going to be present. If the laser is required to provide more services than data and telephony which require a very high SNR and further require a wider error free dynamic range, an optical isolator must be employed. It is important to have a wide dynamic range because when the system is deployed, the signal level can vary over a wide range due to temperature changes in the outside plant or other factors which might increase the loss in the transmission path. Since the fiber degrades the error free dynamic range of the laser, it is especially important to have an optical isolator when the maximum possible error free dynamic range is required. The performance of isolated lasers is considered in the next section.

6.3 Performance of Isolated FP and DFB Lasers with Fiber Spool

An optical isolator for 1.3 μm wavelength was spliced to the lasers. The effect of the optical isolator on the BER versus SNR, BER versus OMI, and SNR versus OMI performance of the lasers was investigated with the presence of the 4.7 dB of fiber spool in the transmission path. The effect of the optical isolator on the noise of the lasers was also investigated.

6.3.1 BER versus SNR

The BER versus SNR performance of the isolated FP and DFB lasers is shown in Figure 17a and Figure 17b, respectively. The BER versus SNR performance of the isolated FP and DFB lasers is similar to the BER versus SNR performance of the unisolated FP and DFB lasers without fiber spool discussed in Section 6.1.2. The isolated FP and DFB lasers had BER of 10^{-9} or less when the SNR was at least 20 dB [Table 6]. The BER performance of these isolated FP lasers deviates more from the theoretical curve than the unisolated lasers. Perhaps some reflections from the splices has increased the IIN.

When an optical isolator was spliced to the FP and DFB lasers, it was found that the spurious reflections from the fiber that were previously seen on the spectrum analyzer when the lasers were unisolated disappeared entirely for all the lasers tested. For the FP and DFB lasers tested, there was no spurious noise induced BER on the order of 10^{-8} until the SNR was at least 19 dB when the OMI was low. This is in contrast to the performance of the unisolated FP and DFB lasers which had a BER on the order of 10^{-8} when the SNR was as high as 39 dB when the OMI was lowered below 1%.

6.3.2 BER versus OMI

The BER versus the OMI performance of the isolated FP and DFB lasers is similar to the BER versus OMI performance of the unisolated FP and DFB lasers without fiber spool discussed in Section 6.1.3.

It can be seen from Figure 18a and Figure 18b that at high OMI, the lasers show BER due to the impairment caused by the clipping of the laser and at low OMI the lasers show BER due to the thermal and shot noise of the optical receiver. The error free dynamic range for the isolated FP and DFB lasers was at least from 0.1% to 12% for all the lasers. The performance of the lasers at high and low OMI is summarized in Table 6.

The optical isolator reduced the reflections from the fiber and other discontinuities in the transmission path from entering the laser. As a result, OMI can be as low as 0.1% without causing errors. This is a factor of 10 lower than the OMI that can be used in the absence of the isolator. The contrast in the BER versus OMI performance of the lasers when they are isolated and unisolated in the presence of the fiber can be seen by looking at Figure 18a and Figure 18b.

As can be seen on Figure 19a and Figure 19b, the optical isolator improved the error free dynamic range of the lasers by at least 15 dB in terms of the RF drive level for both the FP and DFB lasers.

Table 6 shows the maximum and minimum OMI and the corresponding SNR for which error free transmission was observed for the isolated FP and DFB lasers. When no BER was measured in a 2-minute interval, the BER was arbitrarily set to 10^{-9} .The sub-scripts of Mx and Mn next to the RF drive level, OMI, and SNR, indicate the maximum and minimum RF drive level and OMI for which error free transmission was observed and the corresponding SNR.

Table 6: Performance of Isolated Lasers at the Maximum and Minimum OMI With Fiber

Laser (Type)	η_d	RF $Drive_{Mx}$	OMI_{Mx}	SNR_{Mx}	RF $Drive_{Mn}$	OMI_{Mn}	SNR_{Mn}	Dynamic Range
	$\frac{\mu Watts}{mA}$	dBmV	%	dB	dBmV	%	dB	dB
Laser A (FP)	100	41.46	12.1	18.8	-3.54	0.1	18.53	48
Laser B (FP)		41.46	13.6	20.6	2.46	0.17	24.3	40
Laser C (DFB)	120	39.46	13.7	18.5	-10.54	0.074	16.3	51

6.3.3 SNR versus OMI

The OMI versus SNR behavior of the isolated lasers was similar to the OMI versus SNR behavior of the unisolated and uncooled FP and DFB lasers without fiber spool discussed in section 6.1.4. Figure 20a and Figure 20b show the OMI versus SNR performance of the isolated FP and DFB lasers, respectively. The maximum SNR that was measured for the isolated FP and DFB lasers is summarized in Table 7.

Table 7: Maximum SNR of Isolated FP and DFB Lasers With Fiber

Supplier	Laser (Type)	η_d	RF Drive	OMI	Maximum SNR
		$\frac{\mu Watts}{mA}$	dBmV	%	dB
X	Laser A (FP)	100	31.46	4.4	53.5
Y	Laser B (FP)		27.46	2.9	41.2

Table 7: Maximum SNR of Isolated FP and DFB Lasers With Fiber

Supplier	Laser (Type)	η_d	RF Drive	OMI	Maximum SNR
X	Laser C (DFB)	120	31.46	6.6	54.0

When the SNR of the isolated FP and DFB lasers is compared to the SNR of the unisolated FP and DFB lasers, the SNR of the isolated FP and DFB lasers is higher than that of the unisolated lasers when the fiber is present. The reasons the SNR increased when an optical isolator was used will be discussed next.

6.3.4 Effect of Optical Isolator on SNR and Noise

The noise level for isolated FP laser A and isolated DFB laser C decreased by at least 1 dB when compared to the unisolated FP and DFB lasers with fiber spool. The maximum SNR for both lasers increased also. The SNR of FP laser A increased by at least 2 dB and that of DFB laser C increased by as much as 5 dB. Contrary to the results from these two lasers, the SNR of isolated FP laser B decreased by 1 dB. However, this was due to the fact that the laser was biased to give a higher output power when it was unisolated than when it was isolated. Since the RIN is inversely proportional to the emitted power of the laser, the higher the power is the lower the RIN will be.

The performance of the DFB laser improved more with the use of an optical isolator than the FP lasers. This result is similar to the result in section 6.2.5 where it was observed that the noise of the DFB lasers decreased more with the removal of the fiber than the noise of the FP lasers.

6.3.5 Summary of Results for Isolated FP and DFB Lasers

It is seen that the use of an optical isolator in the transmission path improves the error free dynamic range of the lasers dramatically. It is also seen that the SNR of the lasers improves as well. The performance of the isolated FP lasers was as good as the performance of the isolated DFB laser. However, the cost of an isolator can add as much as $250 dollars to the cost of the laser. The cost of an isolated and uncooled DFB laser can be as much as $600 more than the cost of an uncooled and unisolated FP laser [20]. The error free dynamic range improvement that the optical isolator provides for data and telephony transmission should be weighed against increases in the cost of the transmitter due to added cost of the isolator. For services that require a very large error free dynamic range, the use of an optical isolator may be justified.

7. Temperature Measurements

It is known that the SNR of the system decreases when the ambient temperature of the lasers changes. The performance of the lasers when the temperature was changing was tested by putting the lasers in a temperature oven.

7.1 Experimental Details

The lasers tested in the uncooled coaxial packages have a pin photodiode as the back-face monitor. The emitted light from the laser is converted into the backface monitor current. The external quantum efficiency, the coupling efficiency, and the threshold current of the lasers change with temperature. By using the backface monitor as part of a feedback circuit, the emitted power from the laser can be maintained over temperature. The power coupled into the fiber will, however, change owing to the change in coupling efficiency. The photodiode is biased by -5 volts and the backface monitor current is measured by measuring the voltage across a 68Ω resistor that is attached to the photodiode. The bias current is then adjusted manually to maintain a constant monitor current and thus constant emitted power.

Four uncooled FP lasers were tested. Laser W and X were unisolated and laser Y and Z were isolated. These lasers are different from the lasers that were used in the room temperature experiments. The lasers were all biased using the bias-tee circuit such that the optical power at the fiber pigtail was approximately 1030μ Watts. The OMI for all the lasers was first adjusted to give the maximum SNR at room temperature. The temperature was then varied. At each new temperature, measurements were taken after allowing at

least 45 minutes to an hour for the laser to reach thermal equilibrium. The temperature of the laser was measured using a thermocouple that was attached to the laser package. The backface monitor current was then adjusted and the SNR, the RIN, and the BER were measured for each setting of the temperature using the experimental setup described in Section 4.

7.2 SNR as a Function of Temperature

Figure 21 shows the SNR versus temperature for the four lasers that were tested. The SNR of laser W, which is an unisolated FP laser, changed by as much as 9.7 dB when the temperature was increased from 25° C to 85° C and the SNR decreased by 2 dB when the temperature was decreased from 25° C to -40° C. For laser X, the SNR did not change in any significant way with temperature. The SNR just fluctuated around the SNR measured at room temperature by as much as 3 dB. The two other lasers tested showed the same behavior as laser W although the amount of change in the SNR for each laser was different. The SNR of laser Y decreased by 4.3 dB when the temperature increased from 25° C to 85° C, and for the same temperature range laser Z's SNR decreased by 7.7 dB. When the temperature was decreased from 25° C to -40° C, the SNR of laser Y decreased by 3.1 dB. The SNR of laser Z decreased by 3.1 dB overall but showed some fluctuations as the temperature was decreased further. The changes in the SNR were consistent with changes in the signal and noise level as discussed below. For all the lasers tested, sufficient SNR margin was maintained although the SNR decreased as temperature increased. In other words, sufficient SNR margin was maintained over temperature such that error free QPSK transmission was observed.

Table 8: Change in SNR, Signal, Noise, and RIN as a Function of Temperature

Laser (Type)	25°C to 85°C	25°C to 85°C	25°C to 85°C	25°C to 85°C	25°C to -40°C	25°C to -40°C	25°C to -40°C	25°C to -40°C
	ΔSNR (dB)	*ΔSignal* (dB)	*ΔNoise* (dB)	*ΔRIN* (dB)	*ΔSNR* (dB)	*ΔSignal* (dB)	*ΔNoise* (dB)	*ΔRIN* (dB)
W (Unisolated)	-9.7	-3.9	+5.8	+6.3	-2.1	+1.5	+3.6	+3.7
X (Unisolated)	-1.1	-3.6	-2.5	+1.0	+0.7	-0.5	-1.2	-0.6
Y (Isolated)	-4.3	-3.3	+1.0	-3.2	-3.1	0	+3.14	-2.6
Z (Isolated)	-7.7	-2.7	+5.0	+8.8	0	+0.4	+0.4	-0.4

7.2.1 Signal Level as a Function of Temperature

The measured signal level consistently decreased for all the lasers tested when the temperature was increased. Figure 22 shows the change of the signal level with temperature. For example, for laser W, the signal level decreased by 3.9 dB when the temperature was increased from 25°C to 85°C. The rate of change in the signal level was relatively similar for all the lasers. When the temperature was decreased from 25°C to -40°C, the signal level either increased by at most 1.5 dB or remained the same. For example, laser W's signal level increased by 1.5 dB while lasers X, Y, and Z maintained a relatively constant signal level.

The signal level changes with temperature because the external quantum efficiency η_d , the coupling efficiency of the laser to the fiber, and the wavelength of the laser λ all change with temperature.

The external quantum efficiency η_d decreases with increasing temperature. The reasons why the external quantum efficiency decreases with increasing temperature is discussed in detail in Section 2.1. Because of the decrease in the external quantum efficiency, the amplitude of the QPSK signal decreased even though the input RF level to the laser was kept the same. For 1 dB decrease in η_d , the signal level decreases by 2 dB.

The second reason that the signal level decreases when the temperature is increased for the FP lasers is because the wavelength of the laser λ can increase by as much as 0.5 nm/° C [21]. This means that the wavelength of the laser can increase by as much as 30 nm for the temperature range from 25° C to 85° C. The attenuation of the fiber as a function of the wavelength of the laser is given as $Att\left(\frac{dB}{Km}\right) = \frac{C}{\lambda^4}$ where C = 0.35 $\frac{dB}{Km} \bullet \mu m$ for 1.3 μm lasers [22]. The equation assumes that the attenuation of the fiber when the wavelength increases is due to Rayleigh scattering. Since the wavelength of the laser can change by as much as 30 nm from the temperature range from 25° C to 85° C, the attenuation of the fiber can increase by as much as 1.3 dB thereby decreasing the signal level that is measured.

The third factor that affects the signal level is the coupling efficiency of the laser to the fiber which increases with temperature. The increase in the coupling efficiency of the laser, also referred to as tracking error, over the temperature range from -40° C to 85° C is about 1.5 dB in optical power. This can increase the signal level by as much as 3 dB [20].

The fact that the coupling efficiency of the laser to the fiber increases with increasing temperature helps to compensate for the decrease in the signal level due to the decrease in the external quantum efficiency and increased fiber attenuation. However, the increase in the coupling efficiency did not completely offset the decrease in the signal level. For example, the measured signal level of laser W started falling off at a rate of 0.5 dBmV/ 10° C when the temperature was increased from 25° C to 65° C and started falling off more rapidly at a rate of 1 dBmV/10° C from 65° C to 85° C. A similar result was observed for the other lasers. For temperatures greater than 65° C, the more rapid decrease in the signal level might be attributed to the decrease in the external quantum efficiency.

For the temperature range from 25° C to -40° C, the signal level does not change very much for three of the four lasers tested. This is because the decrease in the signal level due to the decrease in the coupling efficiency of the laser and the signal increase due to the lowered attenuation of the fiber roughly cancel out. The external quantum efficiency of the lasers does not increase as much at the lower temperatures [22]. This explains why the measured signal level did not change as much as the temperature decreases from 25° C.

7.2.2 Noise and RIN as a Function of Temperature

The overall noise and total RIN (RIN plus IIN) that were measured for the lasers are more difficult to analyze because they do not show a smooth variation with temperature as the signal. The changes in the overall noise level and RIN as a function of temperature for all the lasers is shown in Figure 23 and Figure 24. The overall noise level and the RIN increased in general. The RIN of the lasers was at least -135 dB/Hz for all the lasers. For laser W, the overall noise and RIN increased by a total of 6 dB when the temperature

increased from 25° C to 85° C and increased by roughly 3.6 dB when the temperature decreased from 25° C to -40° C. The overall noise and RIN of laser X fluctuated by a few dB over the entire temperature range. Laser Y and Z showed pretty much the same behavior as laser W. Laser Y's noise level increased by 1 dB when the temperature increased from 25° C to 85° C. When the temperature was lowered from 25° C to -40° C, the overall noise level and the RIN showed fluctuations of about 2 dB. The RIN also showed fluctuations at the higher temperatures for laser Y. Laser Z showed a similar behavior to laser W although the increase in the noise level was not as much or as smooth as laser W's.

As can be seen from Table 8, the increase in the noise level when the temperature was increased was primarily due to the increase in the RIN for lasers W and Z although in both cases the RIN increased more with temperature change than the overall noise of the system did. However, for lasers X and Y, the change in the noise level was not consistent with the changes in the RIN of the laser over temperature.

The RIN showed a lot more fluctuation than the overall noise did. For the RIN measurements, part of the fluctuation in the result might have arisen from the measurement itself which has a 2 dB error. More careful RIN measurements are needed in order to understand the changes in the overall noise level of the system with temperature.

The increase in the overall noise level and RIN with increasing temperature was expected. When the temperature is increased, the wavelength of the laser changes as has been mentioned before. For multi-longitudinal mode FP lasers, the change in wavelength with temperature along with fiber dispersion causes mode partition noise [see Section 2.1]. Also, the deviation of the laser wavelength from the zero dispersion window around

the 1.3 μm wavelength serves to increase the dispersion of the fiber. Thus, the overall noise increases due to mode partition noise when the temperature is increased or decreased. The RIN of the laser is also expected to increase as the temperature of the laser is increased.

Previous experiments done by Woodward et. al on the temperature dependence of an unisolated and uncooled DFB laser when transmitting an analog signal showed that the SNR for the system decreased by as much as 3.4 dB when the temperature was increased from 25° C to 60° C [3]. In comparison with FP lasers, uncooled DFB lasers also show variations in SNR with temperature. As far as sensitivity to temperature variations is concerned, FP and DFB lasers may have different behavior. Since DFB lasers emit in a single-longitudinal mode, they are not affected by mode partition noise. However, when the temperature is increased for DFB lasers, the gain spectrum of the laser shifts. Further experiments will be conducted to compare the performance of the FP and DFB lasers when the temperature changes.

8. Summary and Conclusion

Detailed measurements of unisolated and uncooled FP and DFB lasers were done for use in return path applications in HFC networks. It is found that these lasers can be used for error free transmission of QPSK over a wide range of OMI. Both the unisolated DFB and FP lasers measured had a maximum SNR greater than 40 dB. There was not a significant difference in the maximum signal to noise ratio for both the DFB and FP lasers. Overall, both types of lasers are suitable for transmission of QPSK modulated data and telephony services. However, since DFB lasers are more sensitive to reflections from the fiber than FP lasers and more expensive, FP lasers provide a satisfactory solution meeting performance and cost targets.

The effect of fiber on OMI ranges for error free transmission was also investigated. It was seen that the performance of the lasers was limited by spurious reflections caused by the fiber. It is shown that the use of an optical isolator significantly reduced these spurious reflections and the error free OMI range was significantly improved. The error free dynamic range was improved by at least 15 dB for all the lasers studied.

When the ambient temperature of the uncooled and isolated or unisolated FP lasers changed, the SNR decreased with increasing temperature. However, the SNR did not decrease enough to cause degradation in BER performance for all the lasers tested. The SNR for all the lasers was above 39 dB over the temperature range from -40° C to 85° C. There was no major difference in the performance of isolated or unisolated FP lasers when the temperature was changed.

The above results show, that uncooled FP lasers would work very well in transmitting QPSK modulated data and/or telephony services over a wide range of temperatures. While the SNR was maintained such that no BER penalty was observed, some applications may require minimal variations in signal levels.

One possible way of maintaining constant signal level when the temperature is changing would be to add a thermal compensating circuit. The level of thermal compensation required would depend on the signal and noise level changes and it should be such that clipping of the laser does not occur. A simple thermal compensating circuit may be easily implemented in the transmitter which would provide a cheaper solution than using a thermoelectric cooler.

Appendix A. Attached Plots of Spurious Noise as it Appears on the Spectrum Analyzer

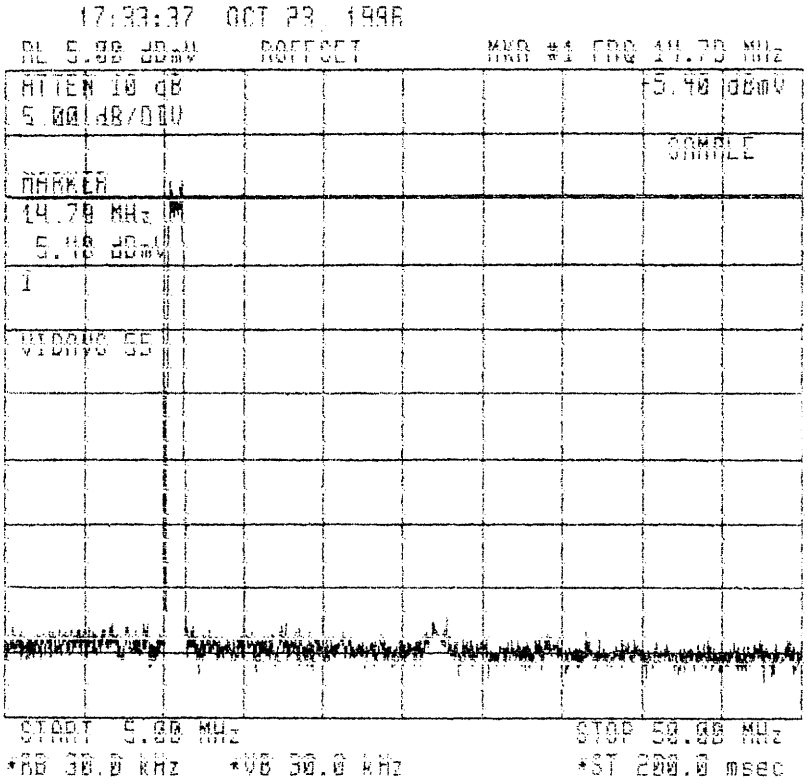

Carrier Power
= -5.40 dBmV

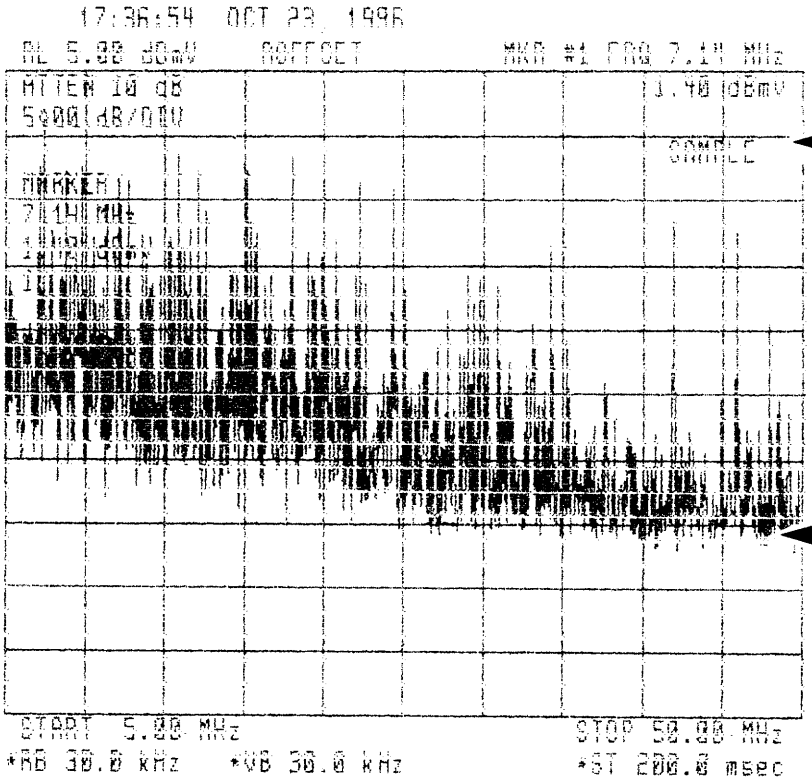

Maximum Spike
= 1.40 dBmV

Noise Floor
= -22.39 dBmV

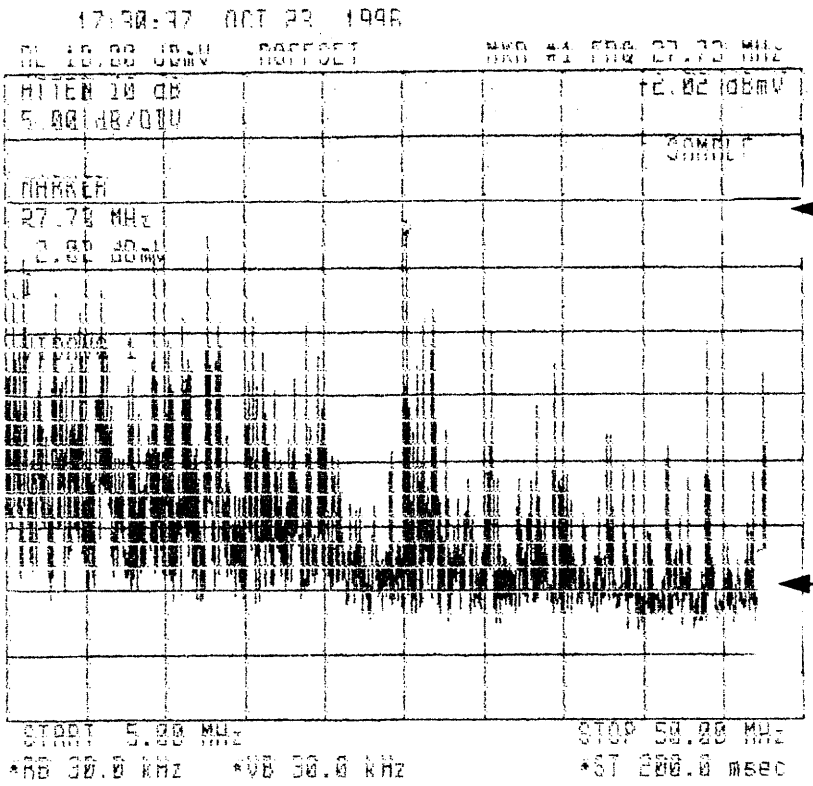

Maximum Spike
= -2.82 dBmV

Noise Floor
= -22 dBmV

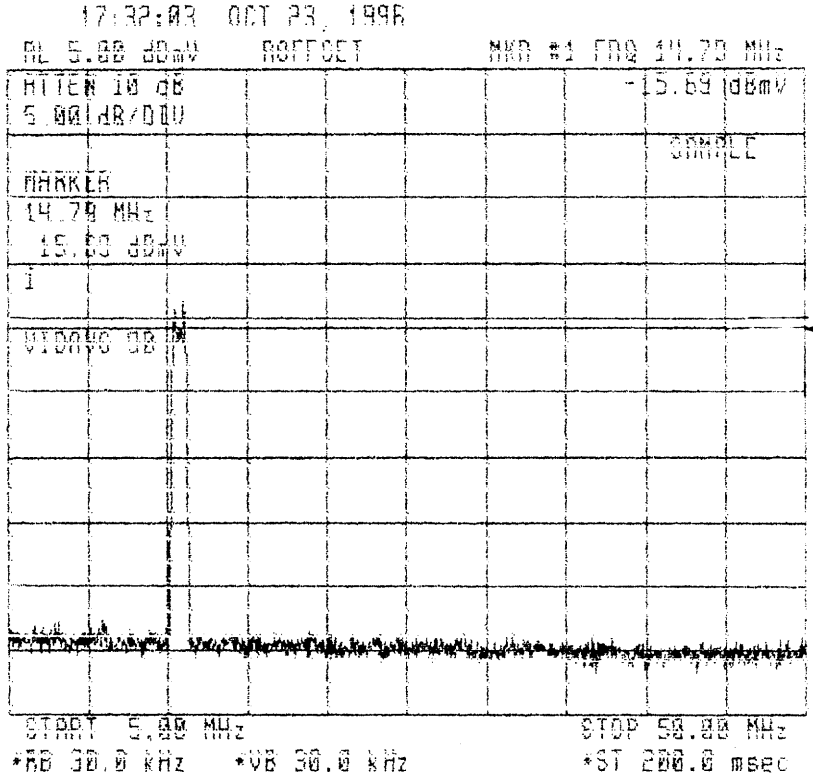

Carrier Power
= -15.69 dBmV

Appendix B. Attached Plots of the BER versus SNR, BER versus OMI, BER versus RF Drive Level, and SNR versus OMI for Unisolated and Uncooled FP and DFB Lasers With and Without Fiber Spool

Figure 8
BER vs SNR for QPSK Mod and Demod Back-to-Back

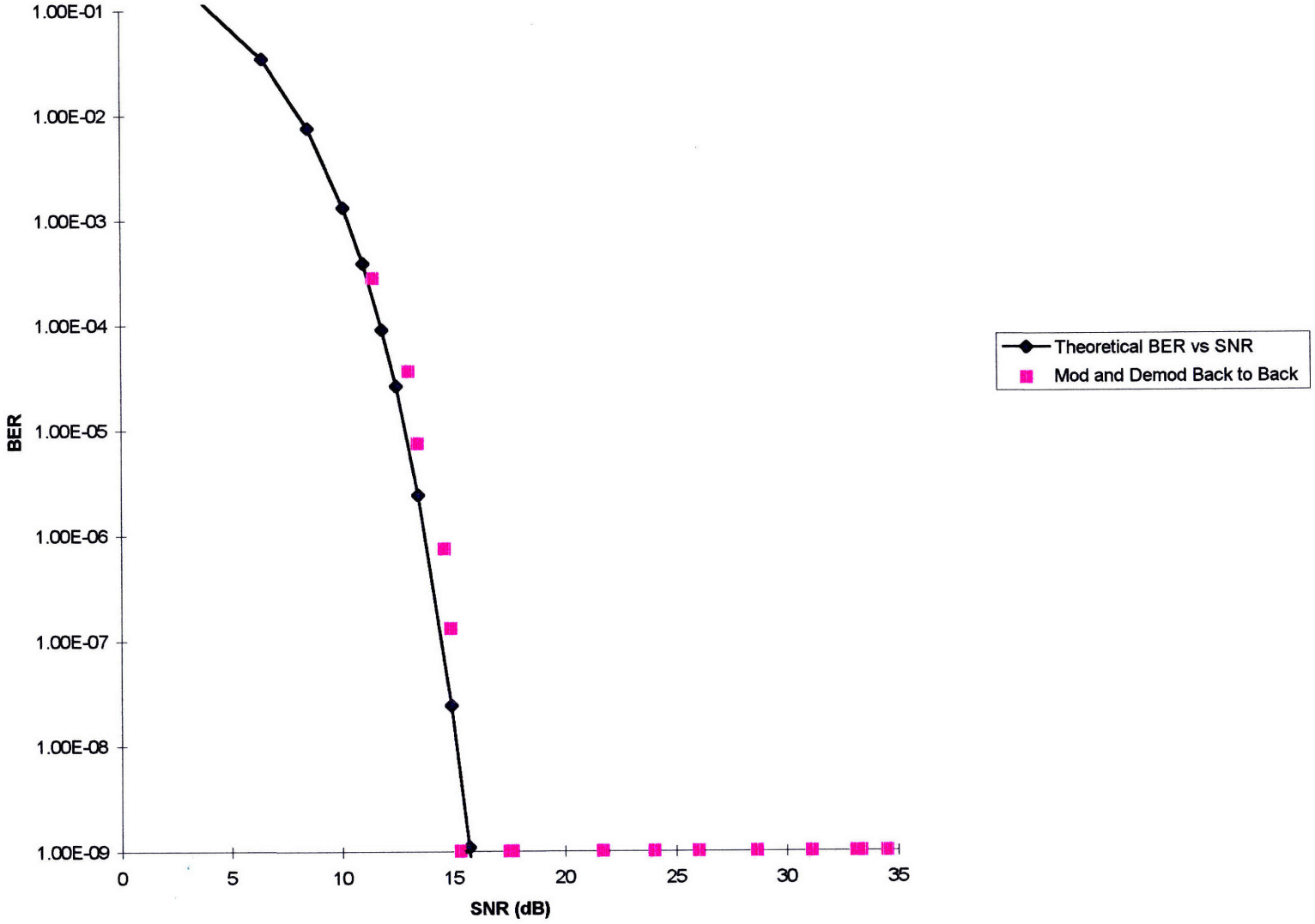

Figure 9a

BER vs SNR For Unisolated FP Lasers Without Fiber

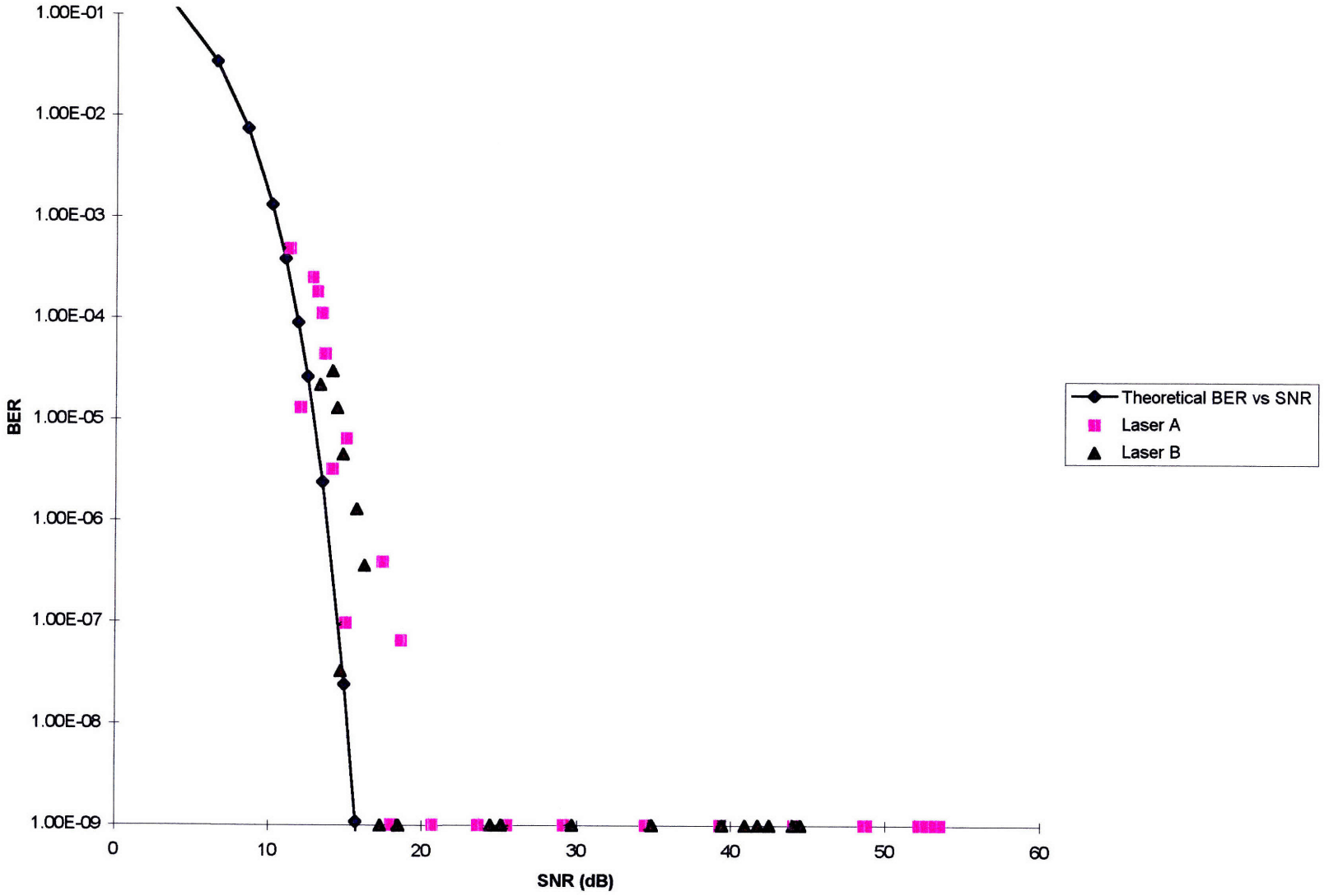

Figure 9b

BER vs SNR for Unisolated DFB Lasers Without Fiber

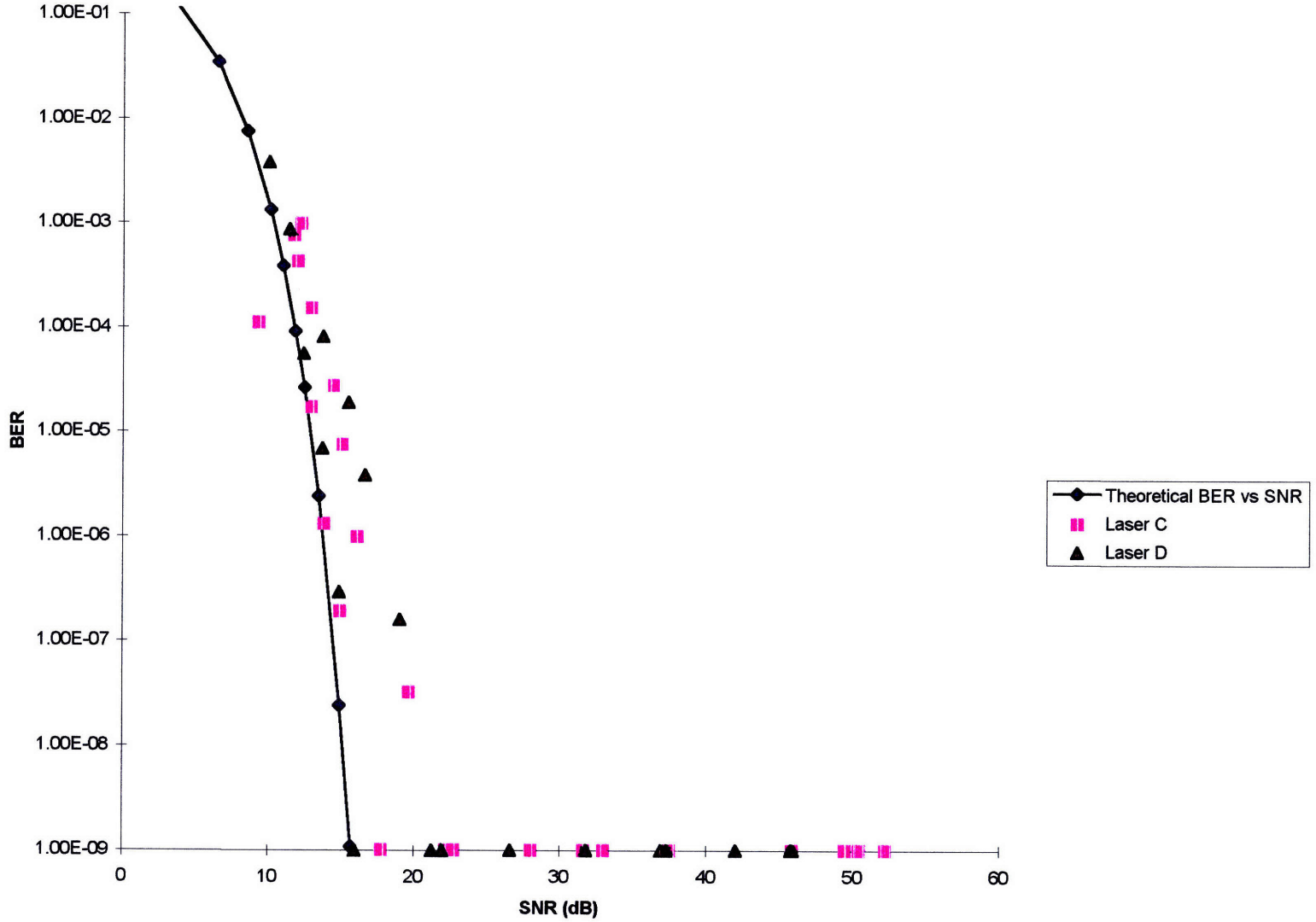

Figure 10a
BER vs OMI for Unisolated FP Lasers Without Fiber

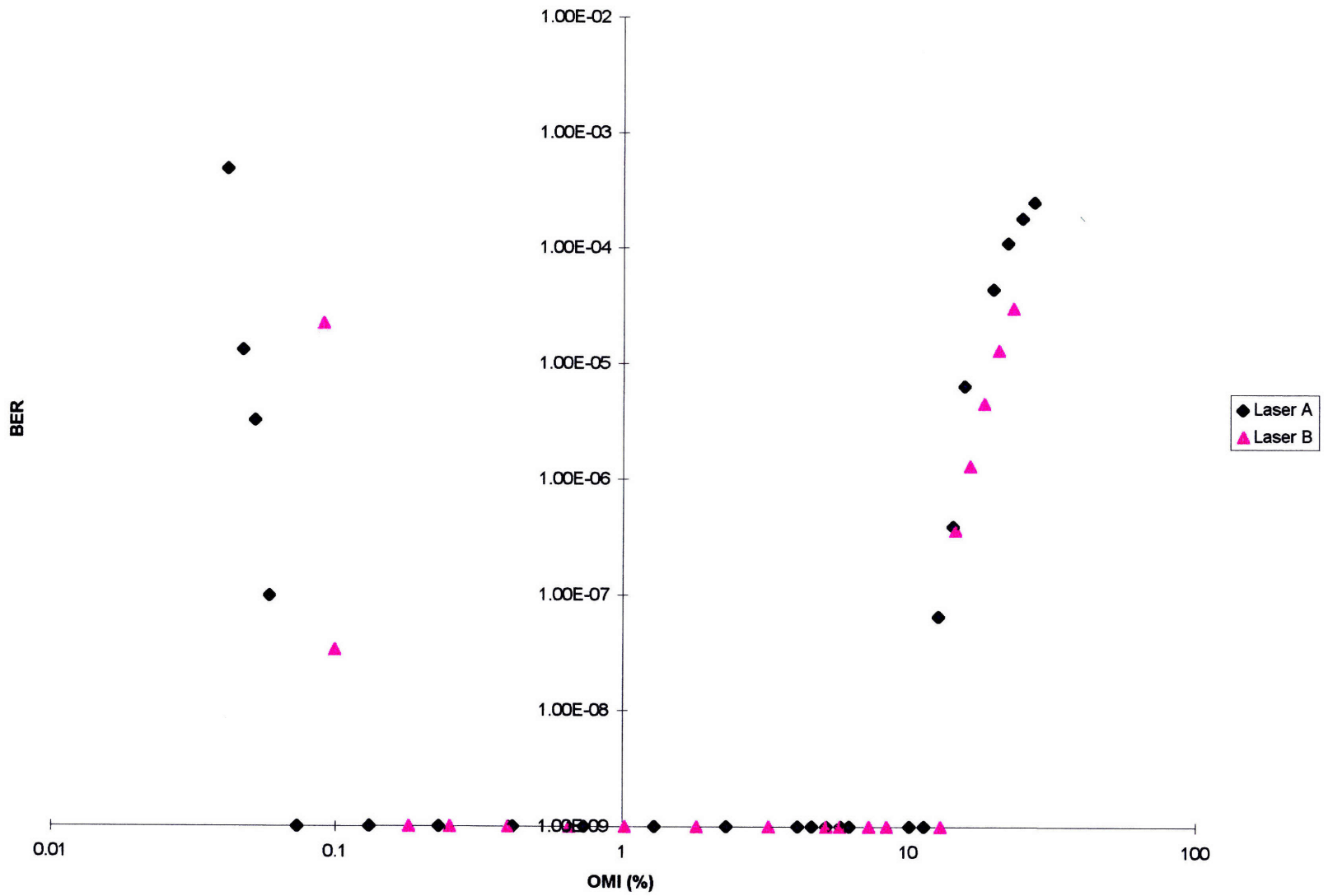

Figure 10b

BER vs OMI for Unisolated DFB Lasers Without Fiber

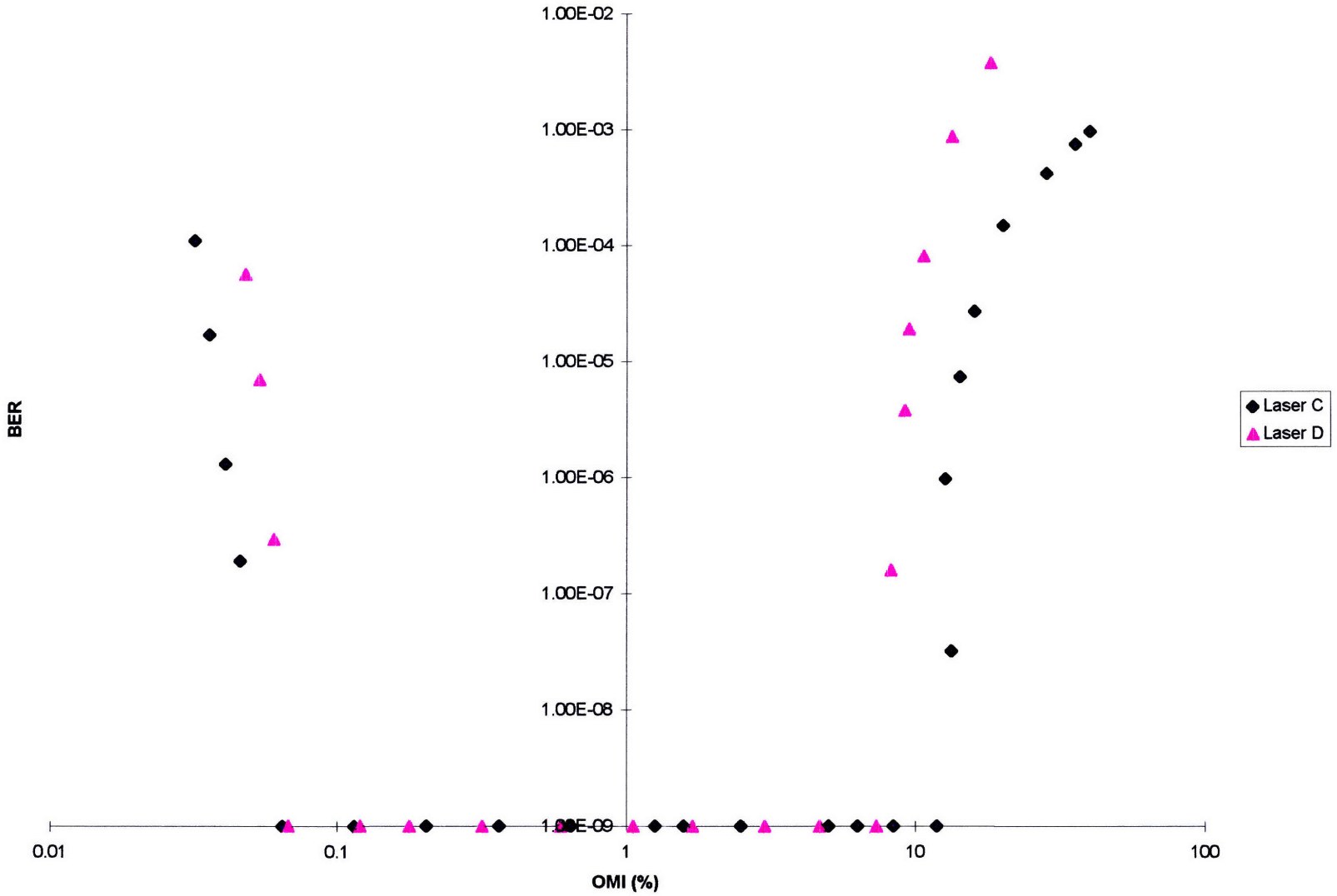

Figure 11a

BER vs RF Drive Level for Unisolated FP Lasers Without Fiber

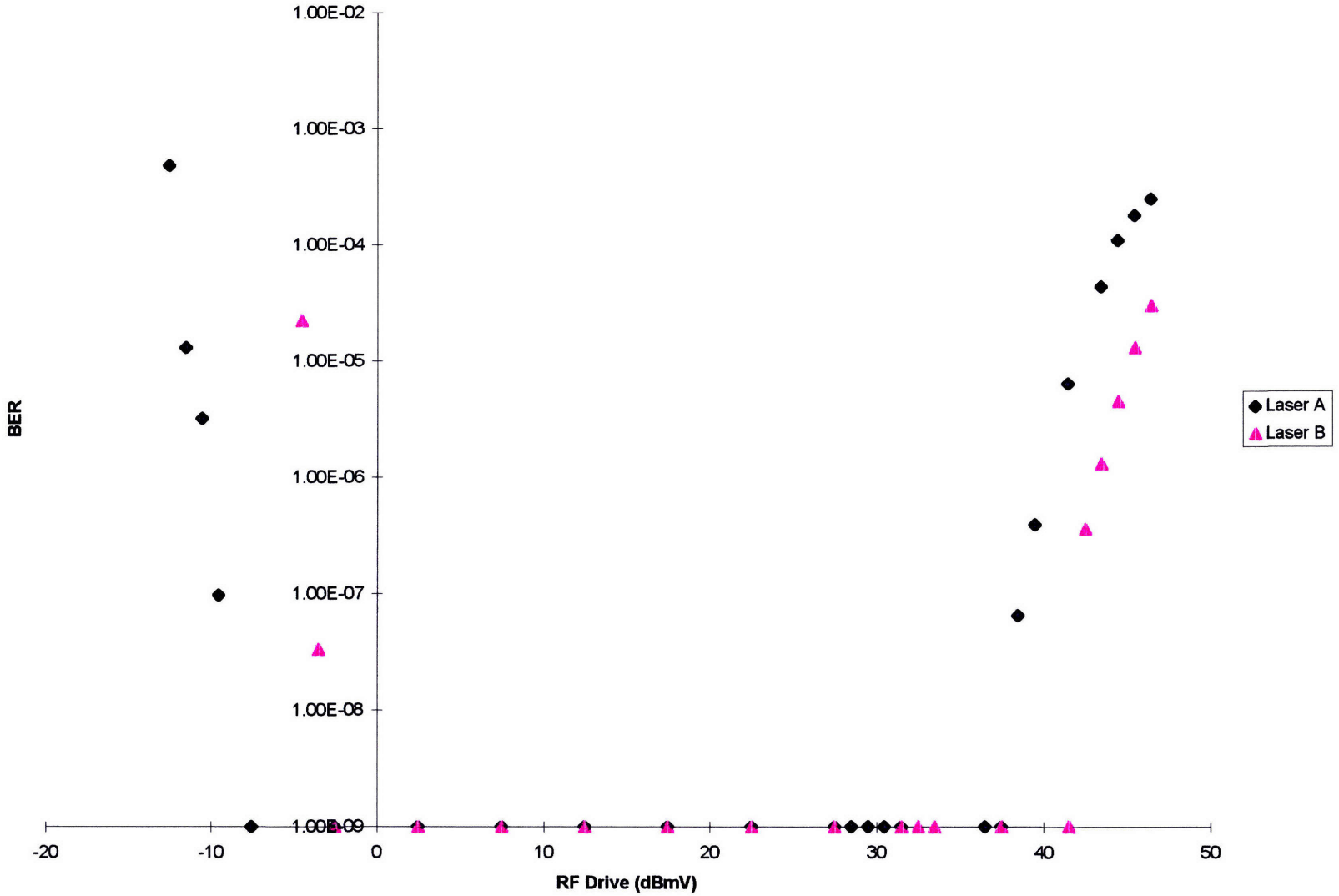

Figure 11b

BER vs RF Drive Level for Unisolated DFB Lasers Without Fiber

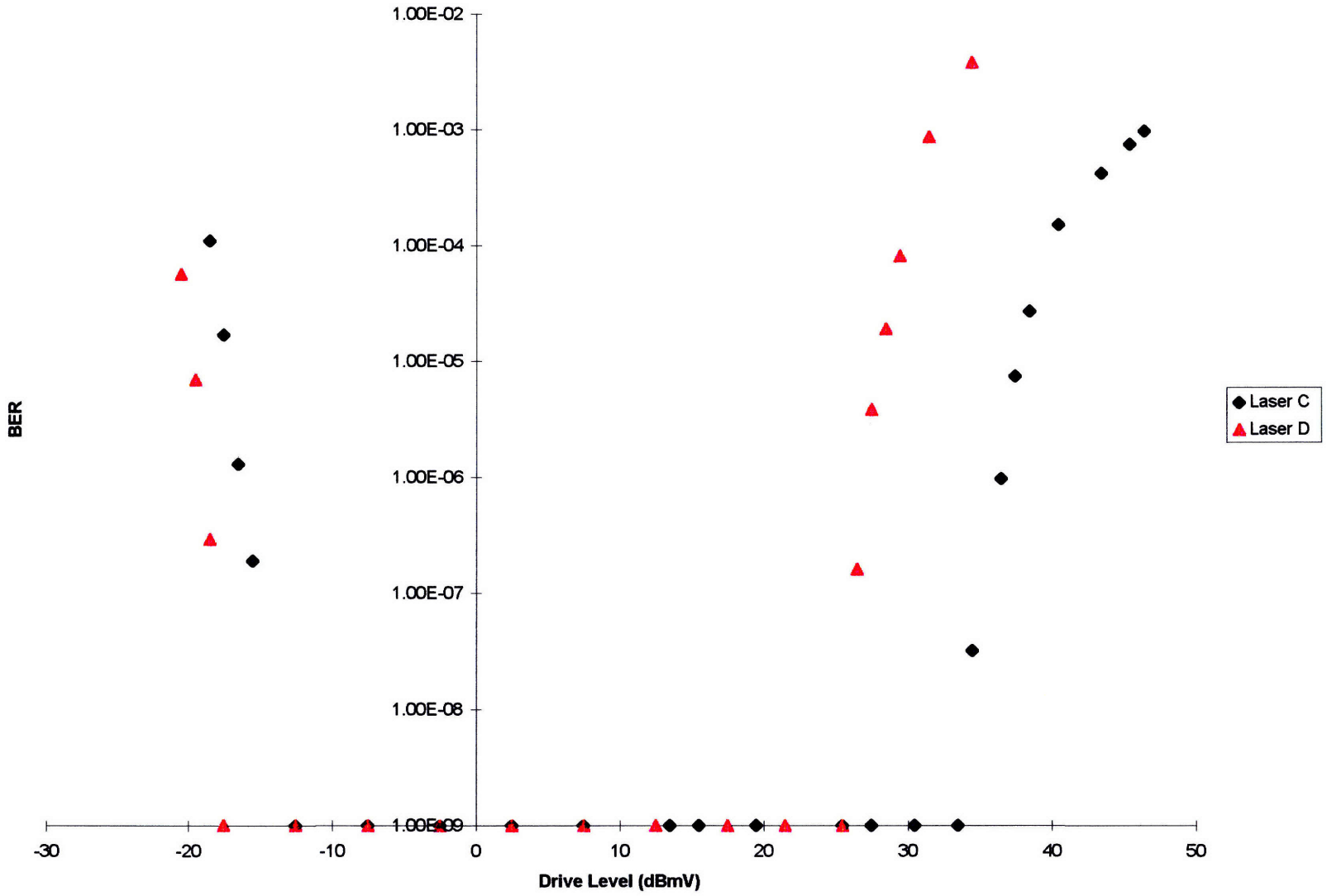

Figure 12a

SNR vs OMI for Unisolated FP Lasers Without Fiber

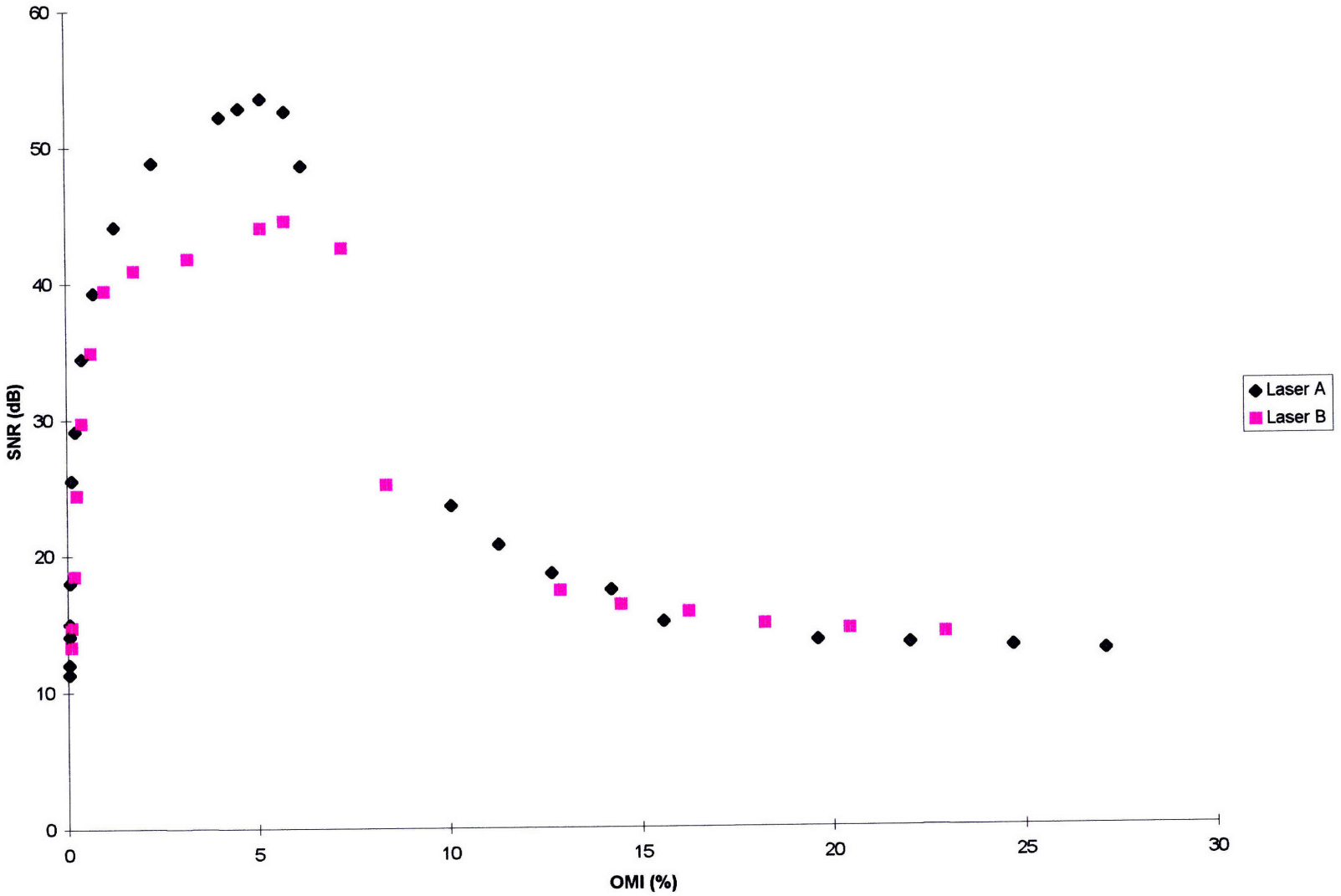

Figure 12b
SNR vs OMI for Unisolated DFB Lasers Without Fiber

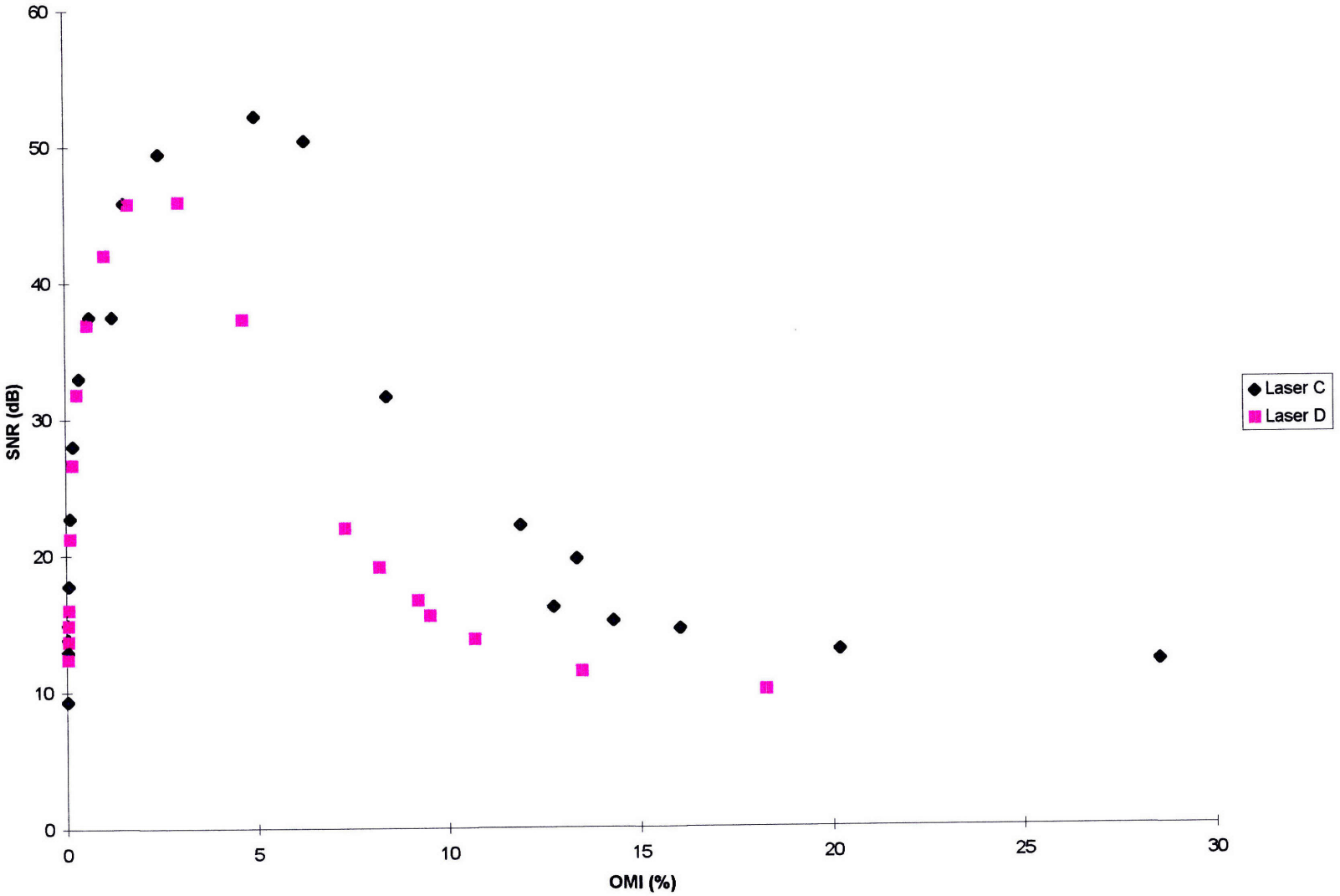

Figure 13a

BER vs SNR For Unisolated FP Lasers With Fiber

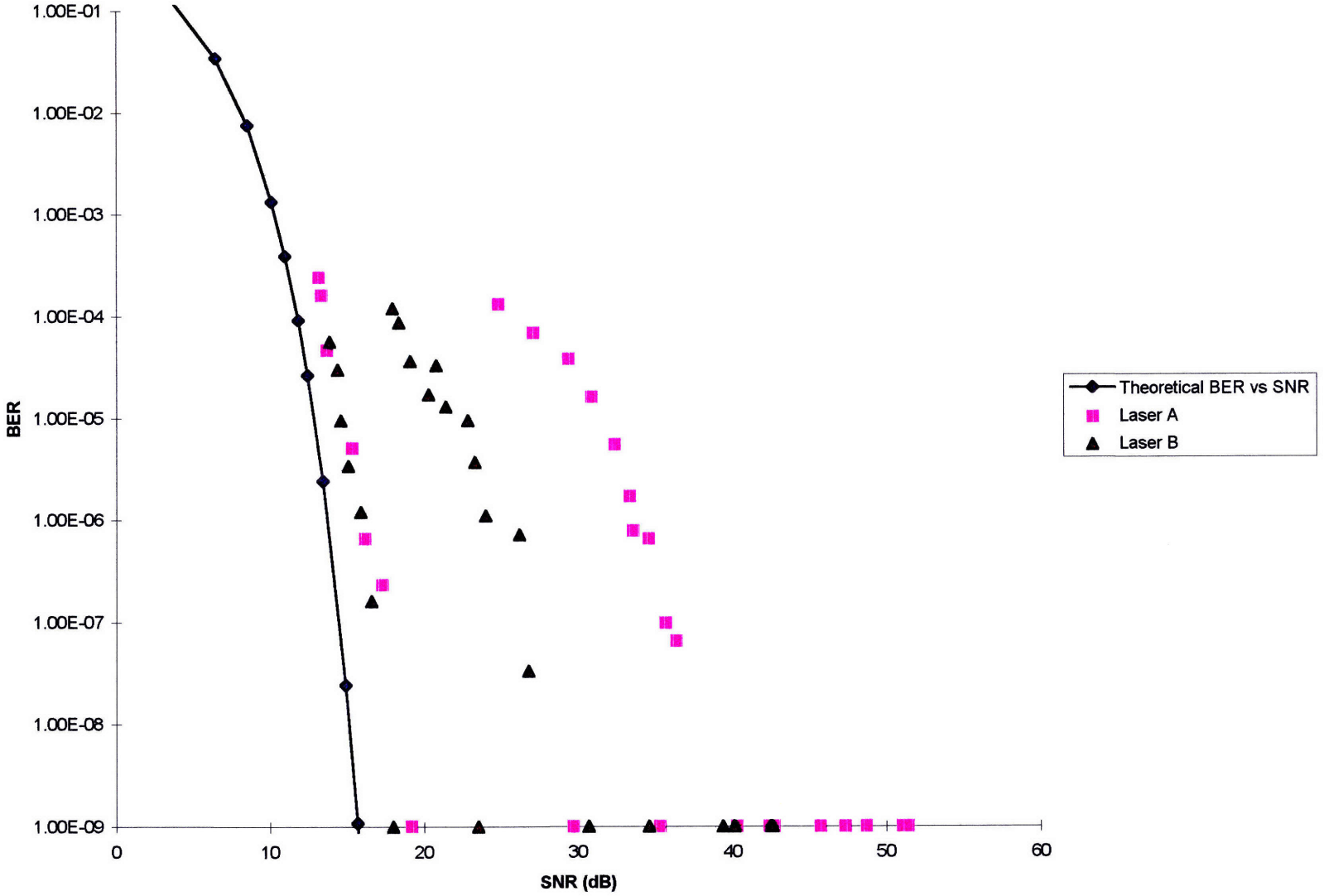

Figure 13b

BER vs SNR for Unisolated DFB Lasers With Fiber

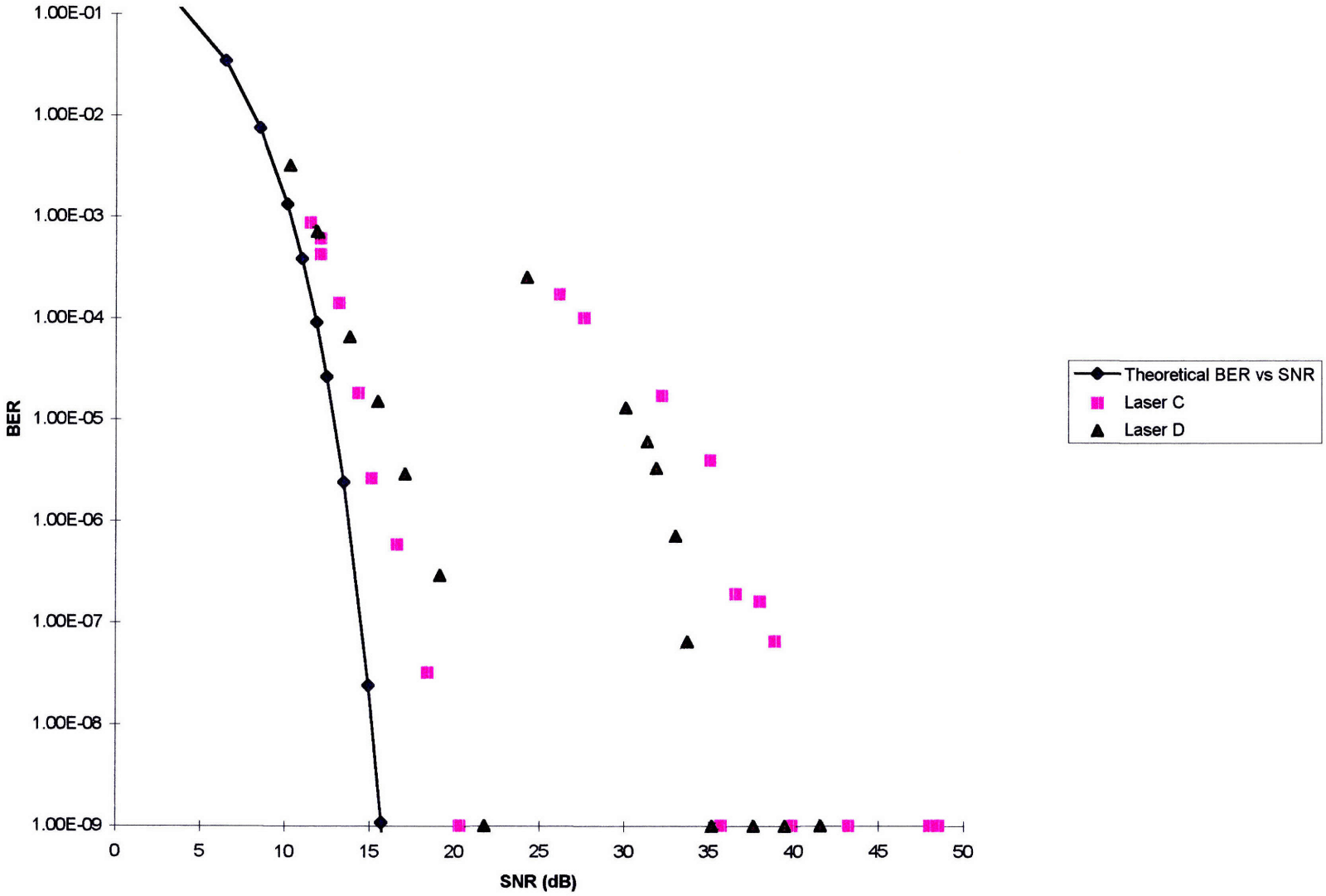

Figure 14a
BER vs OMI for Unisolated FP Lasers

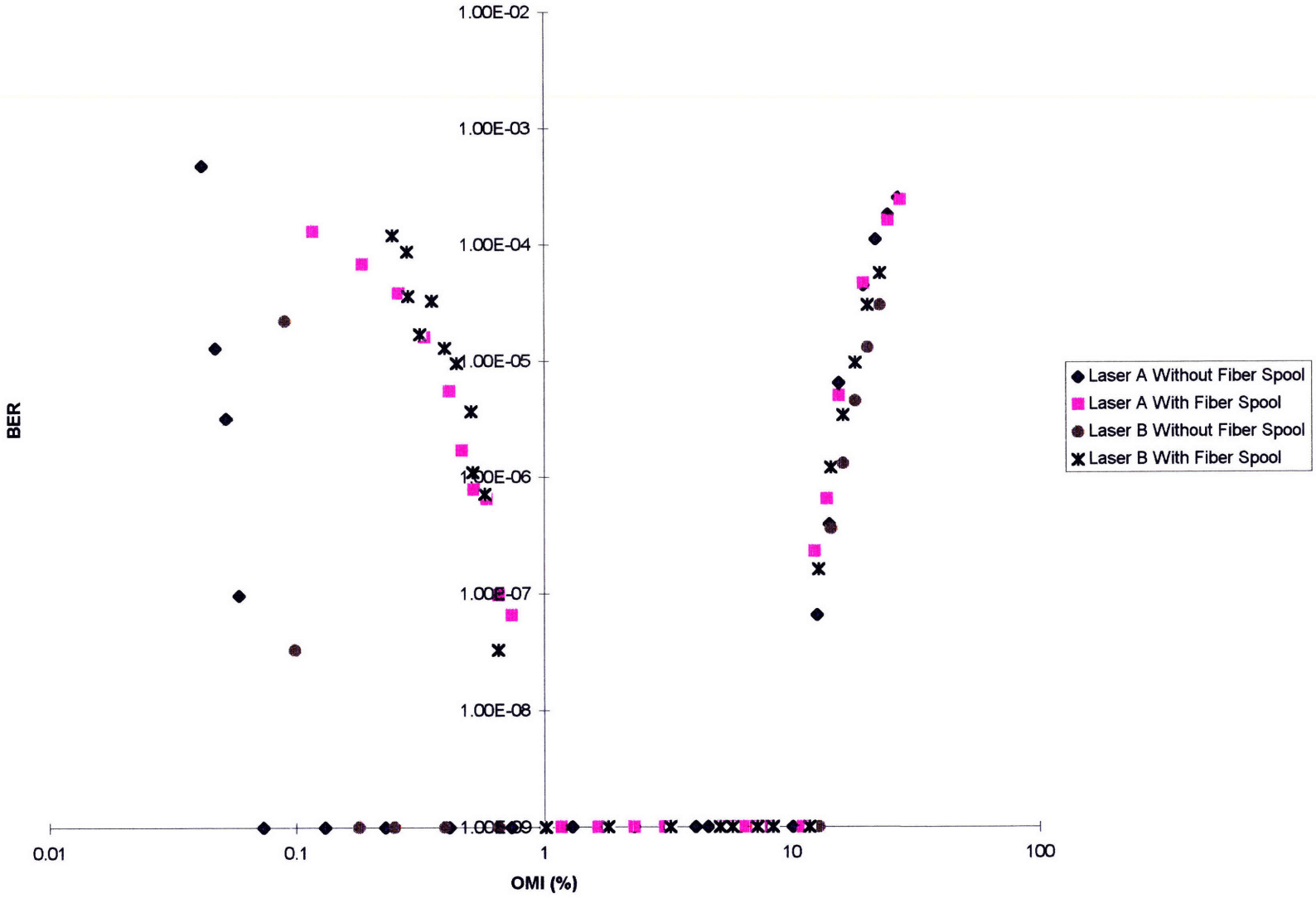

Figure 14b
BER vs OMI for Unisolated DFB Lasers

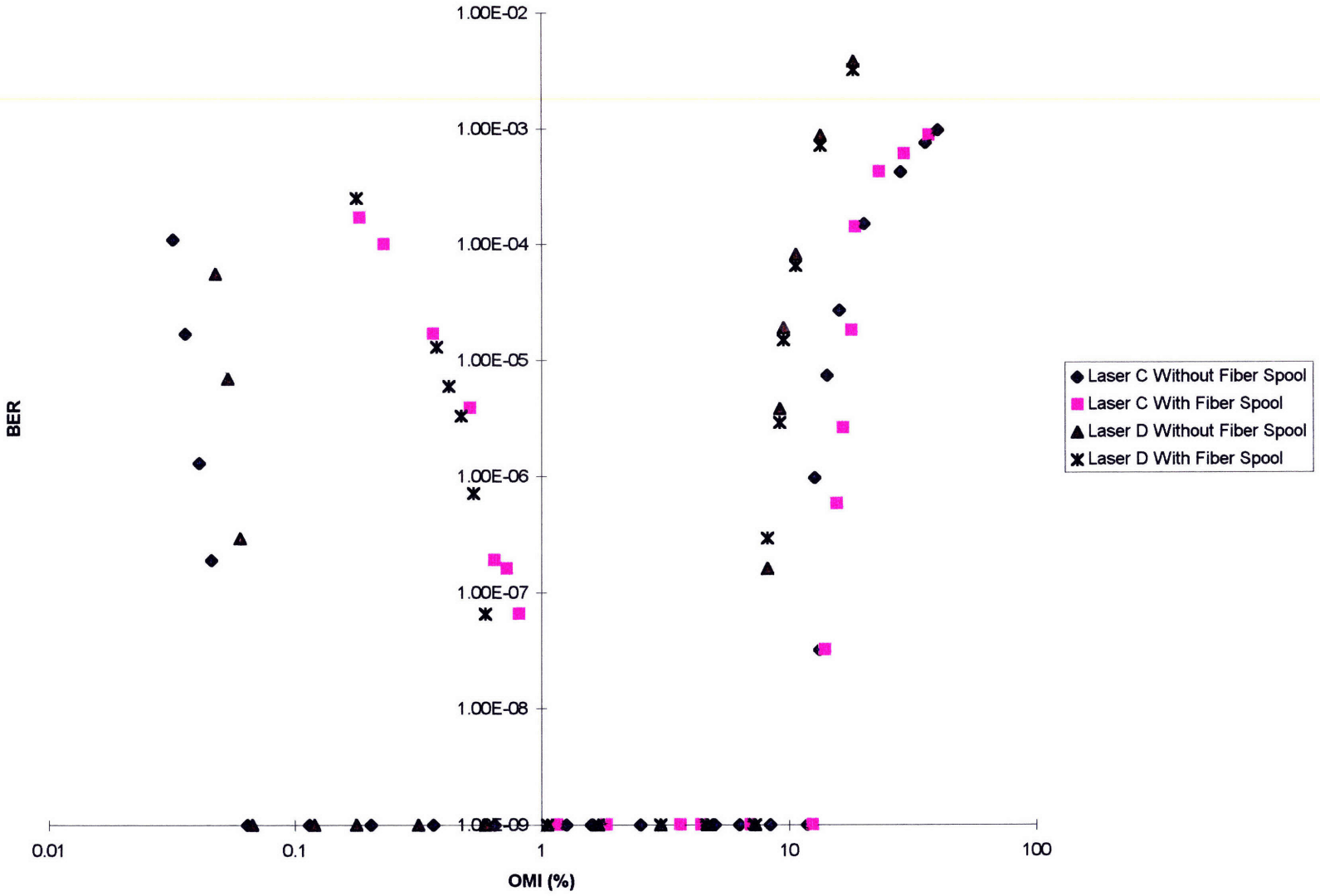

Figure 15a
BER vs RF Drive Level for Unisolated FP Lasers

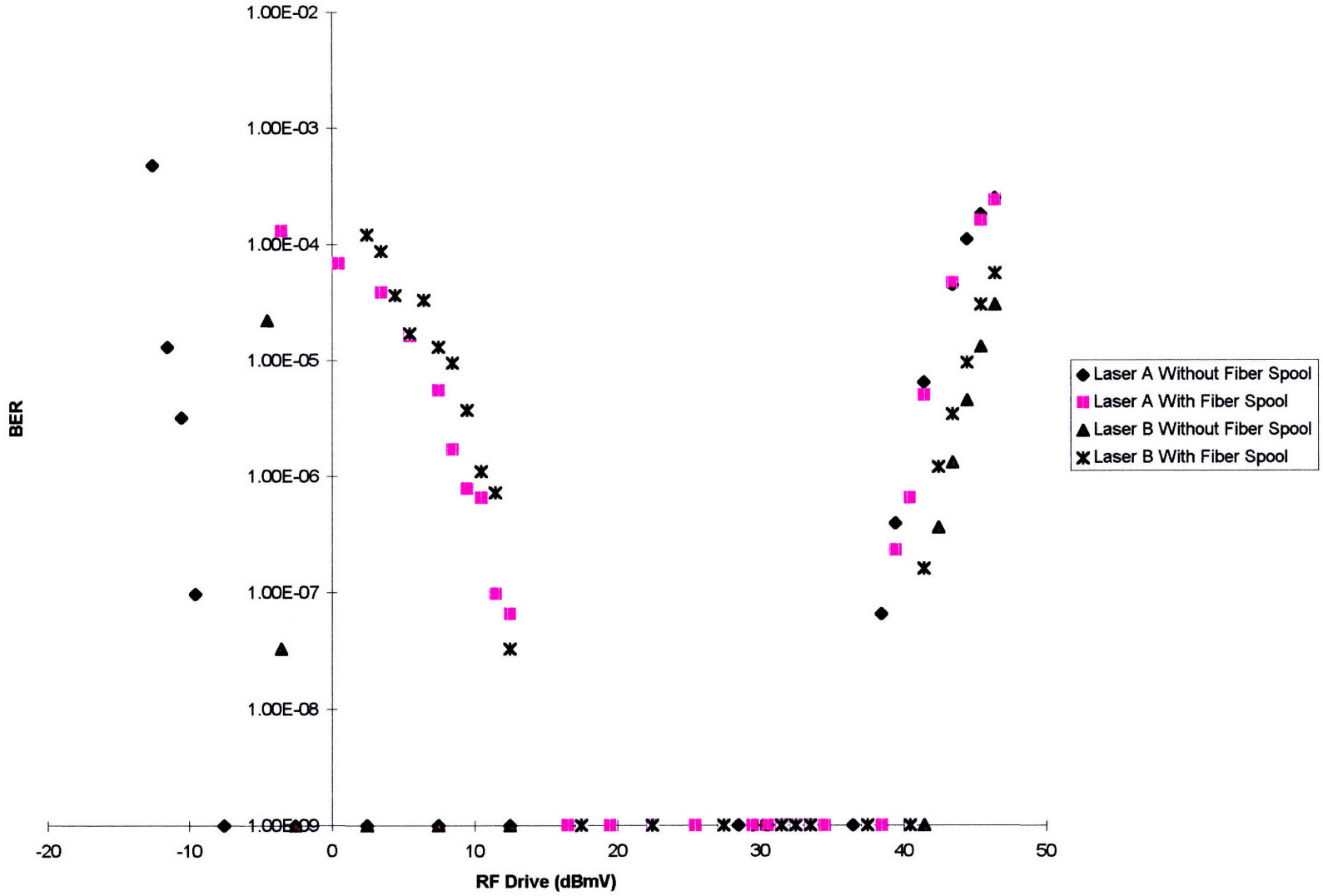

Figure 15b

BER vs RF Drive Level for Unisolated DFB Lasers

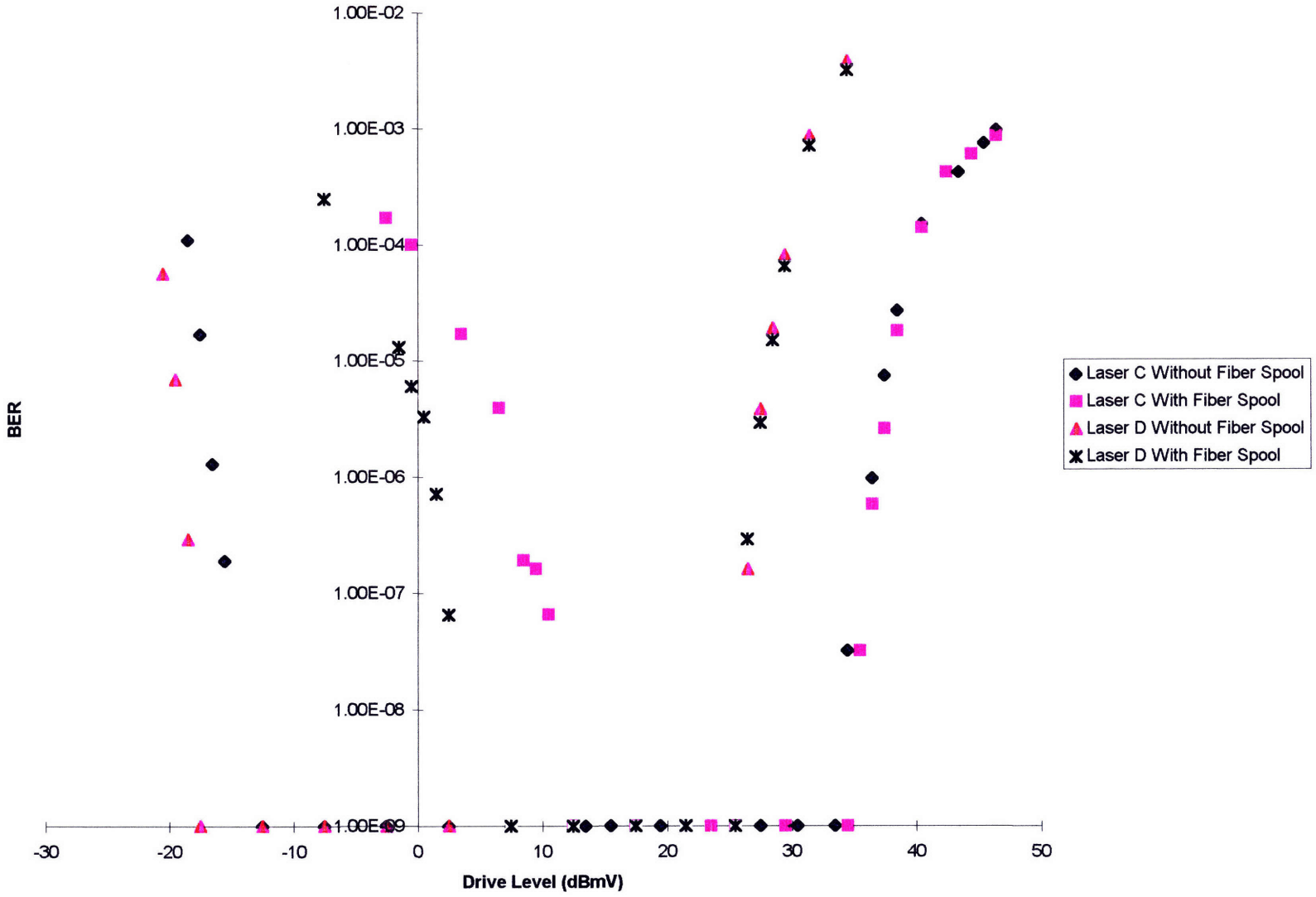

Figure 16a

SNR vs OMI For Unisolated FP Lasers With Fiber

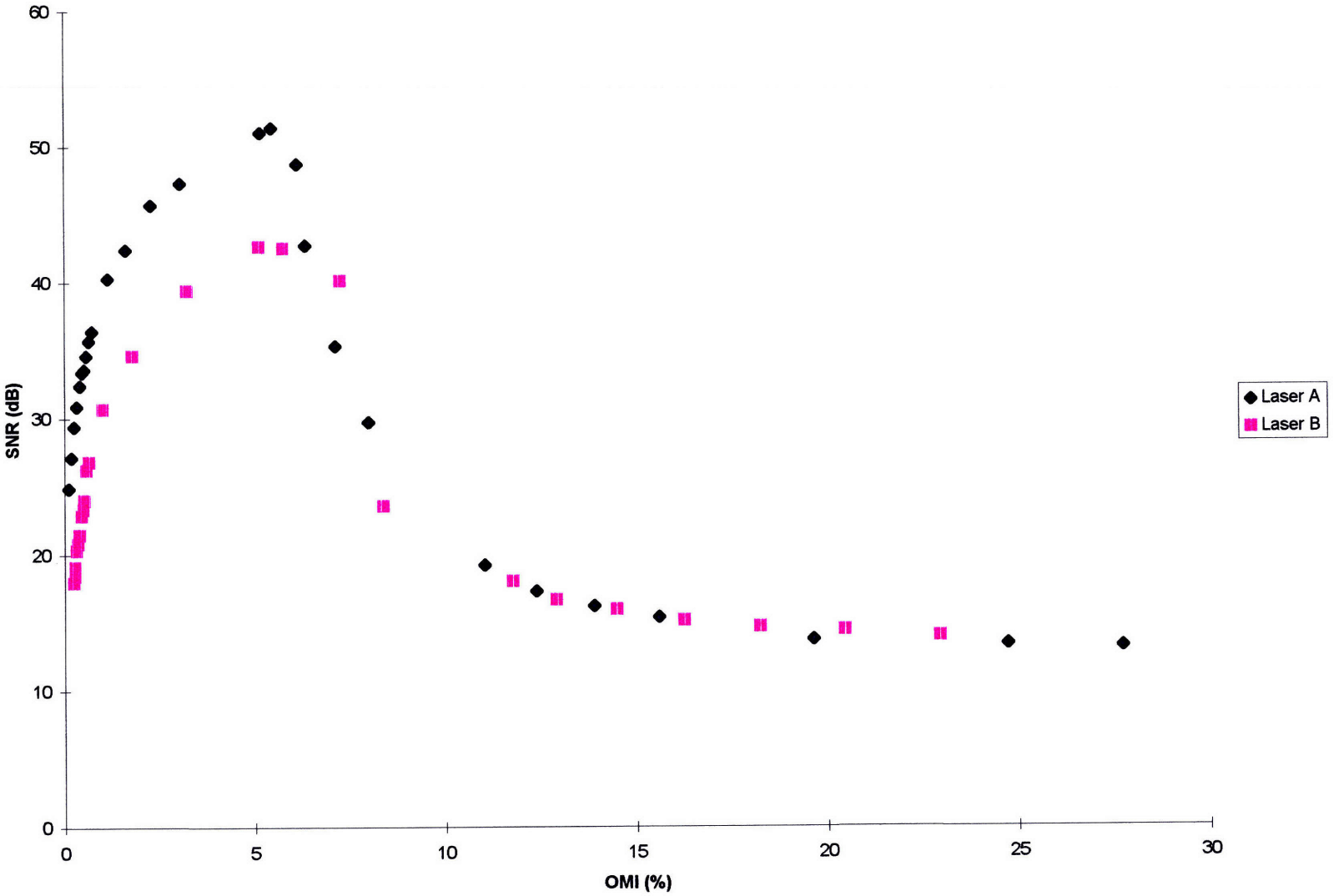

Figure 16b

SNR vs OMI For Unisolated DFB Lasers With Fiber

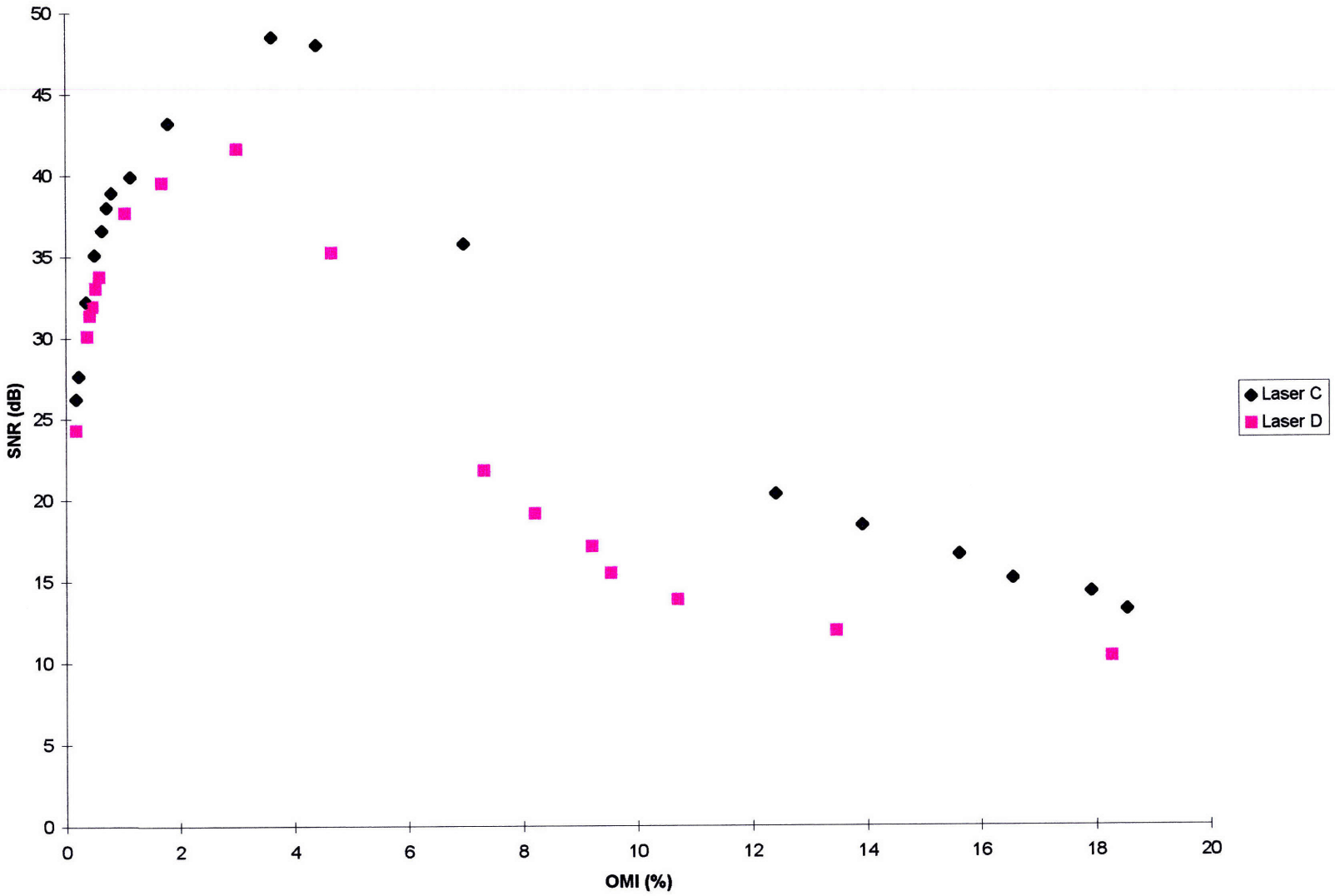

Figure 17a
BER vs SNR for Isolated FP Lasers With Fiber

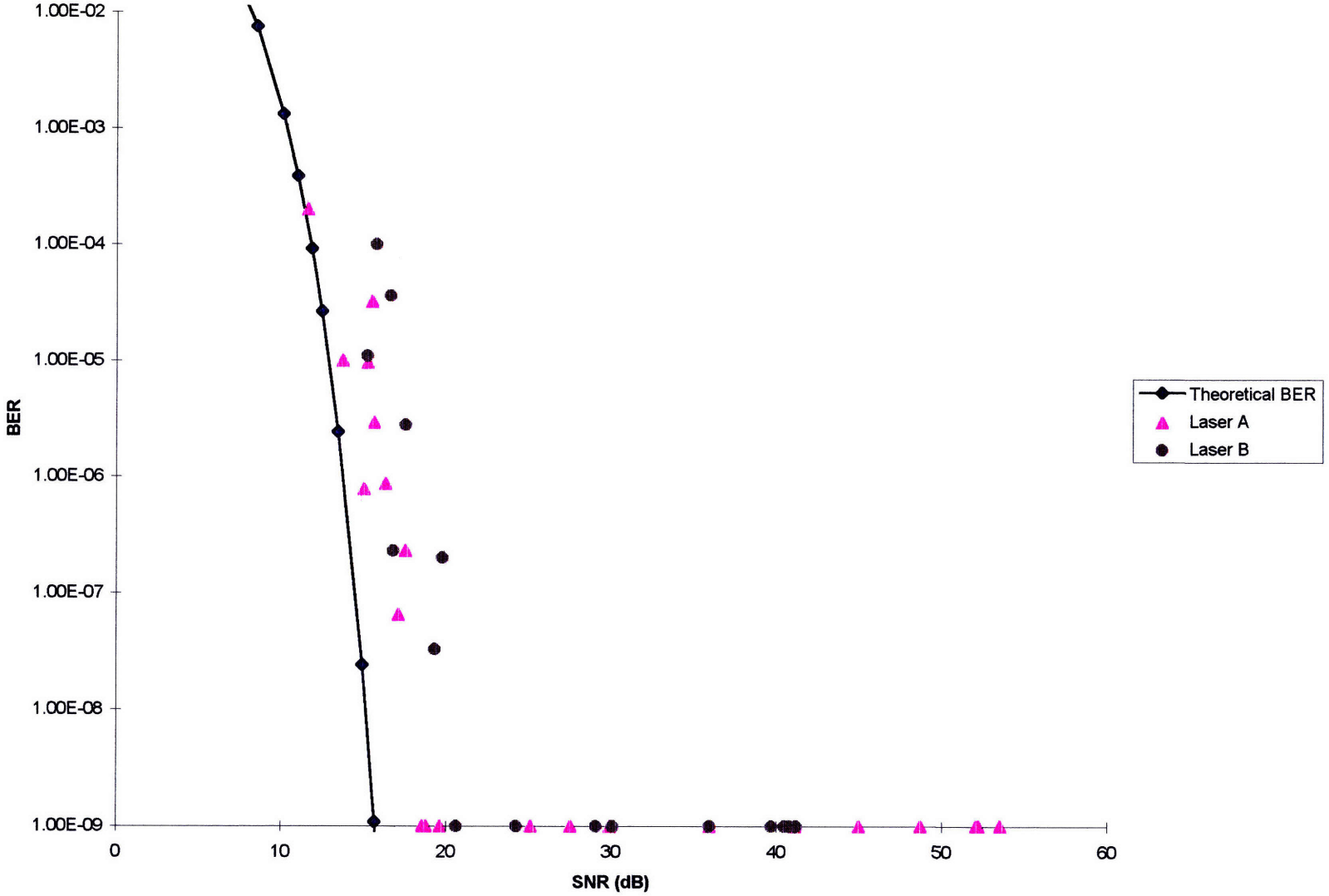

Figure 17b
BER vs SNR for Isolated DFB Laser With Fiber

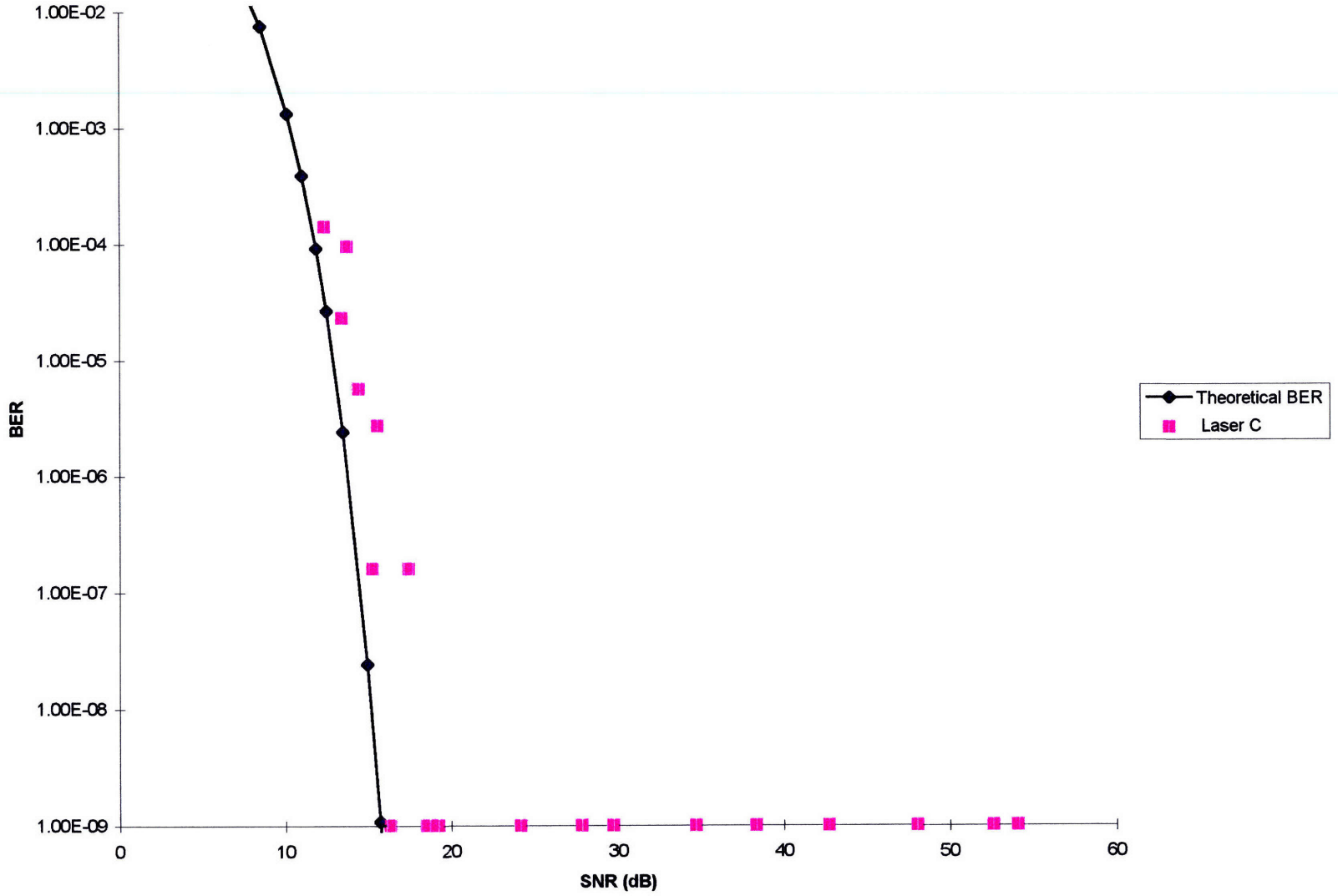

Figure 18a

BER vs OMI for Isolated and Unisolated FP Lasers With Fiber

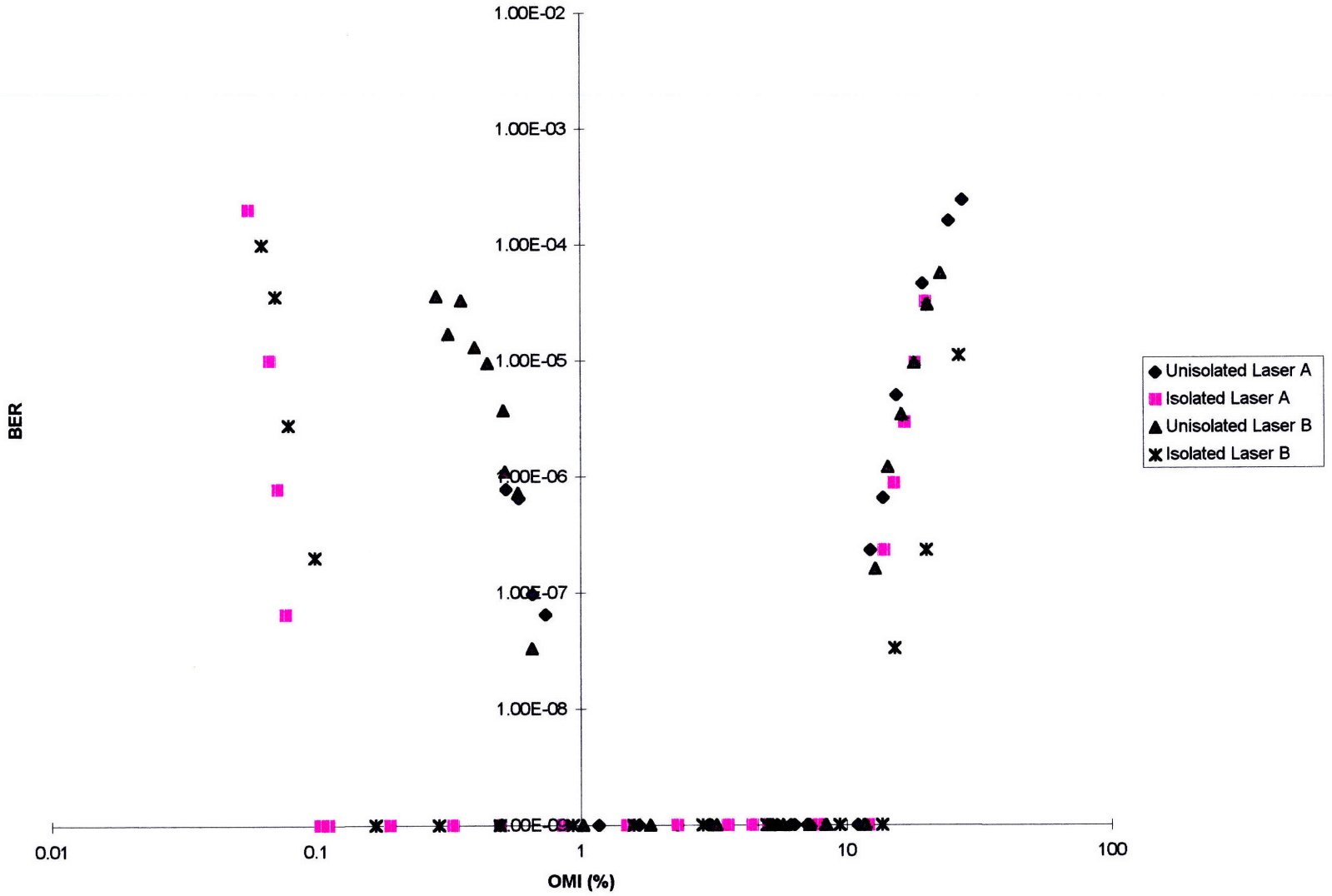

Figure 18b

BER vs OMI for Isolated and Unisolated DFB Laser With Fiber

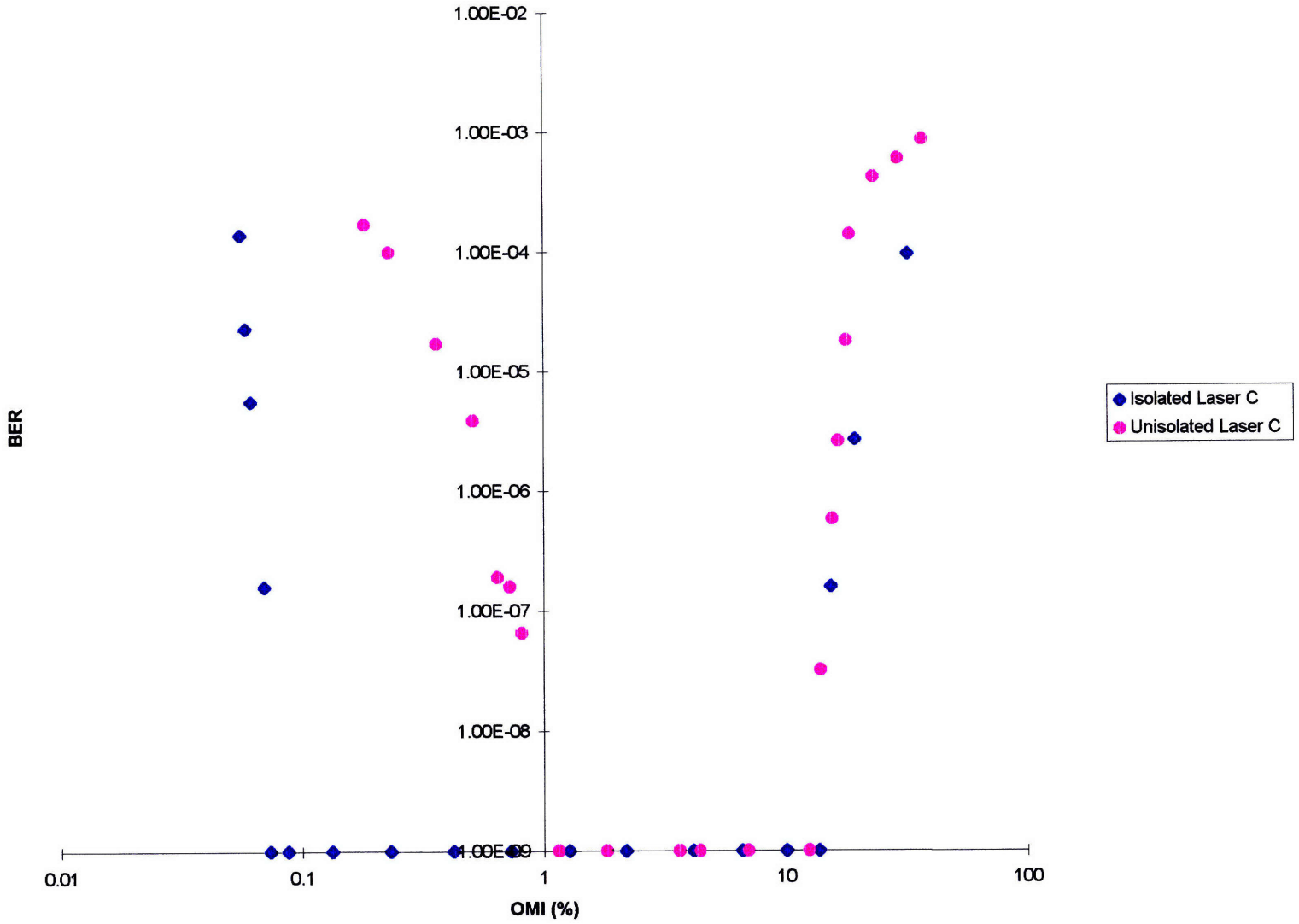

Figure 19a
BER vs RF Drive Level for Isolated and Unisolated FP Lasers With Fiber

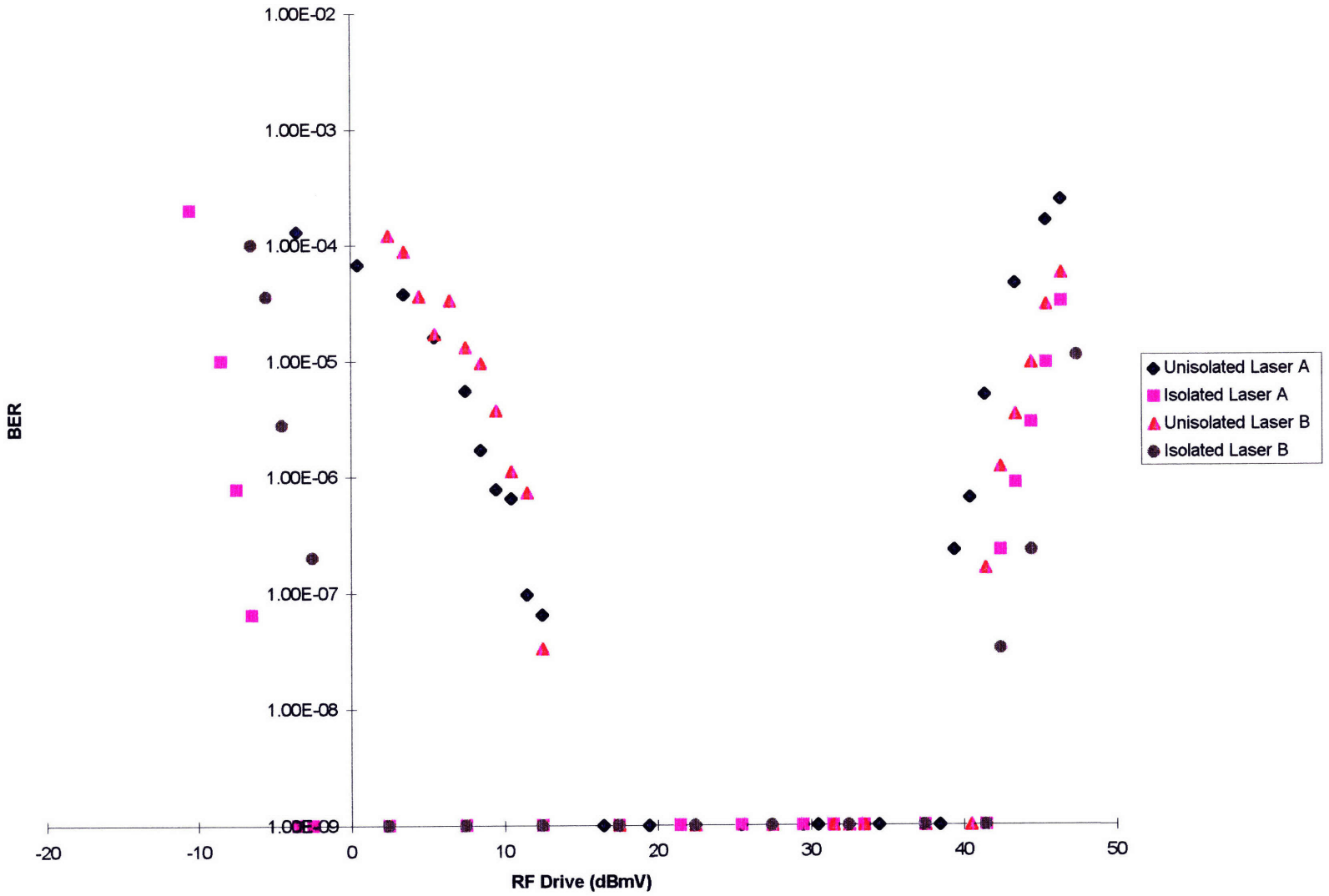

Figure 19b

BER vs RF Drive Level for Isolated and Unisolated DFB Laser With Fiber

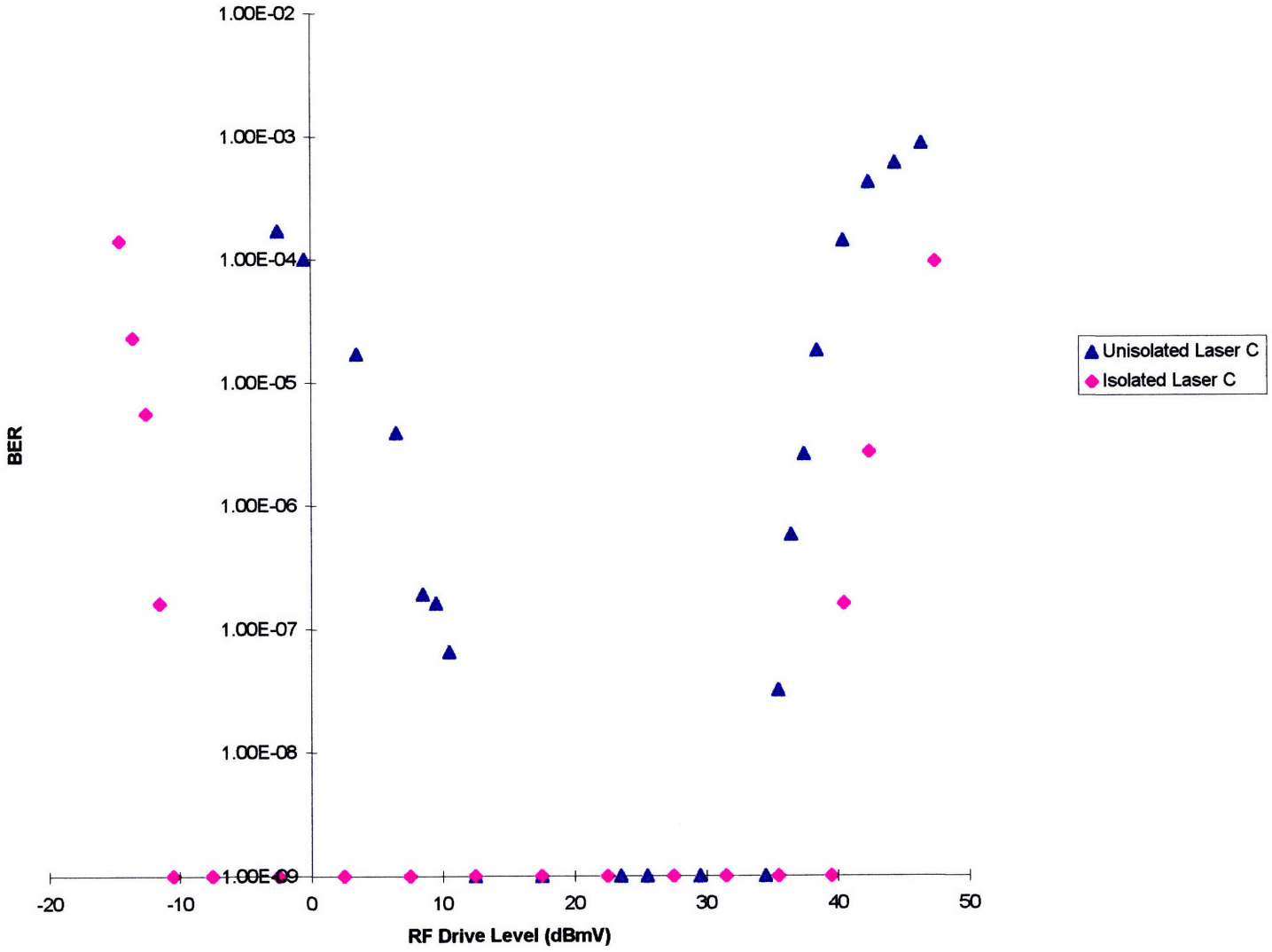

Figure 20a

SNR vs OMI for Isolated FP Lasers With Fiber

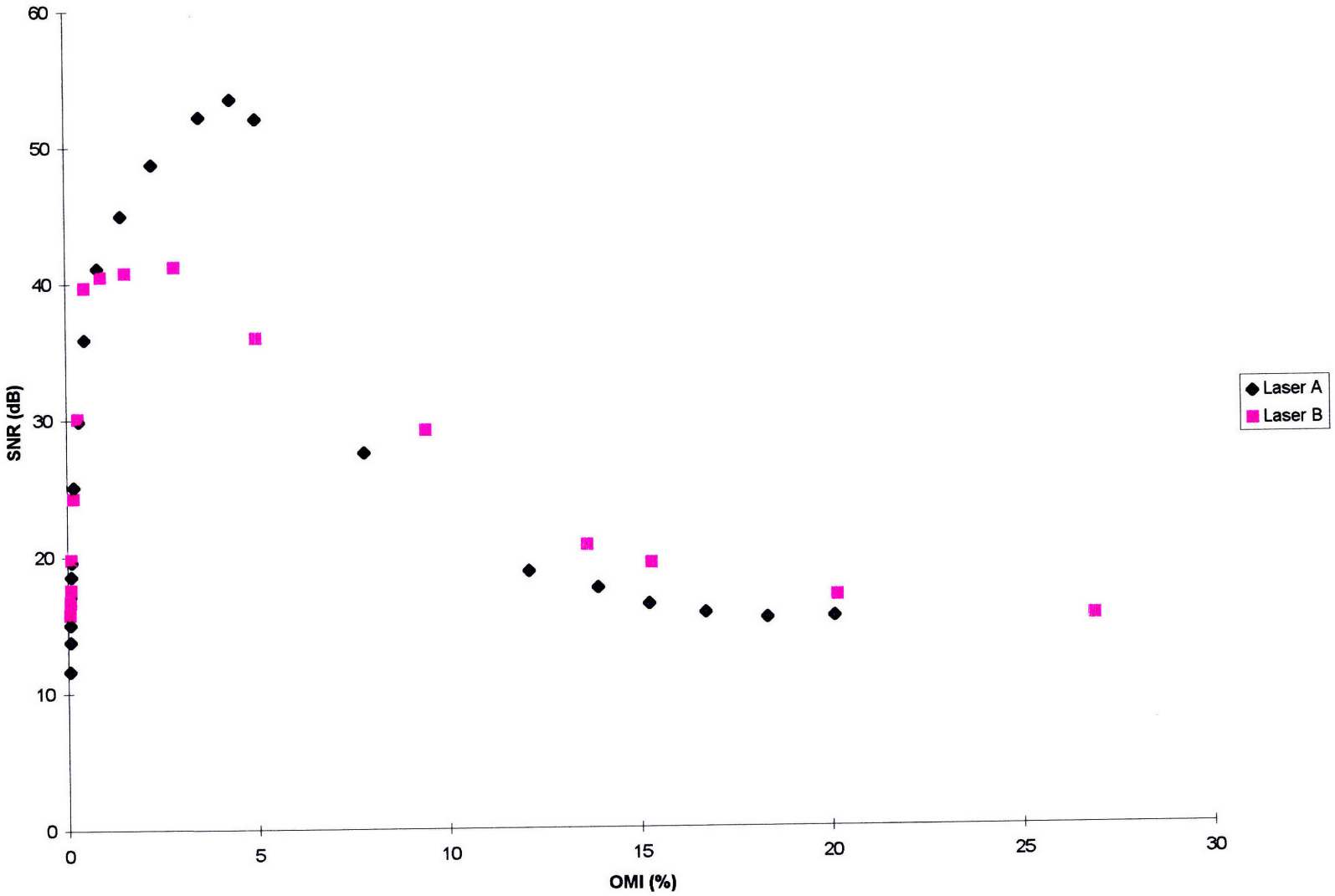

Figure 20b

SNR vs OMI for Isolated DFB Laser With Fiber

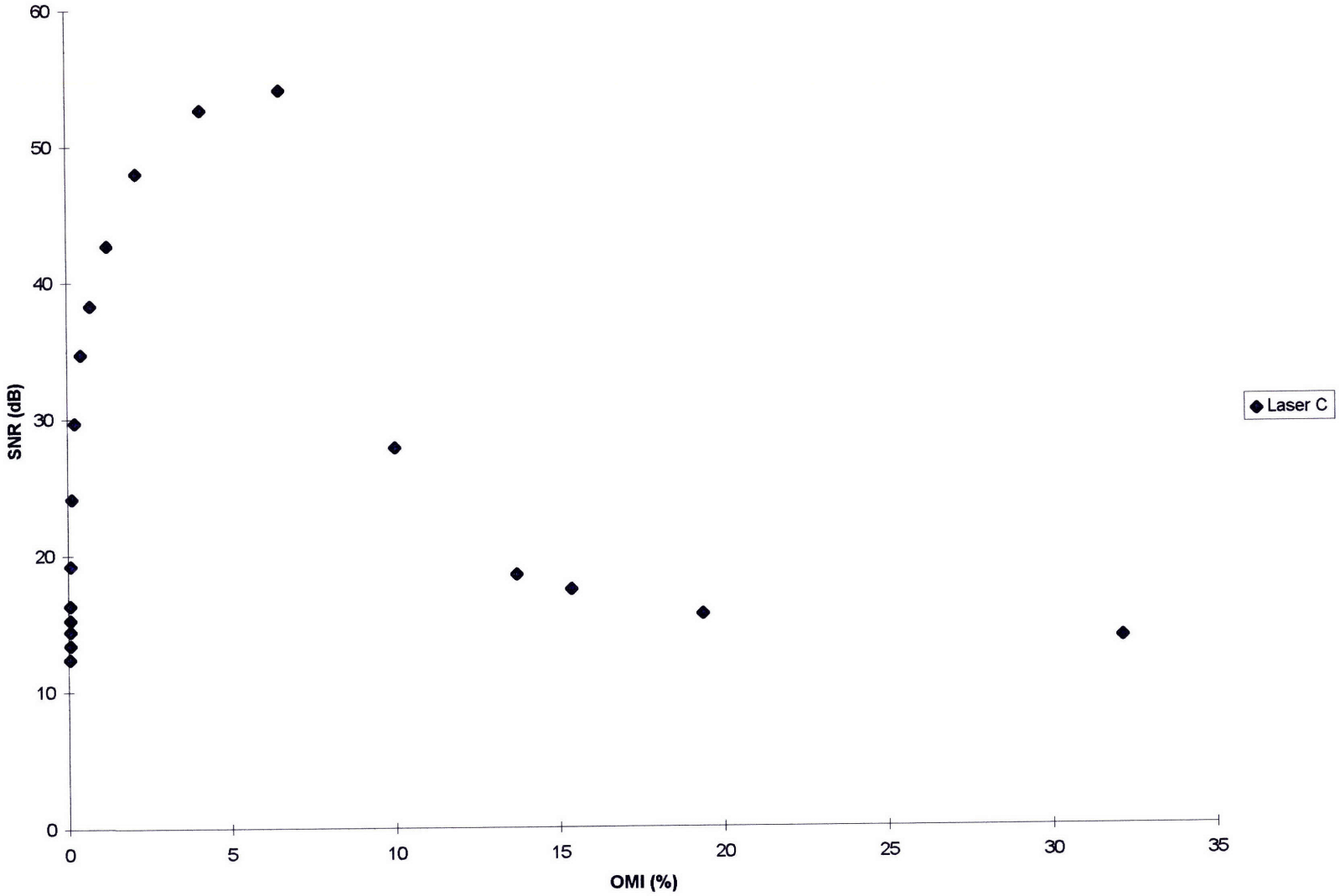

Appendix C. Attached Plots of the SNR, Signal Level, Noise, and RIN as a Function of Temperature

Figure 21

SNR vs Temperature for Isolated and Unisolated FP Lasers

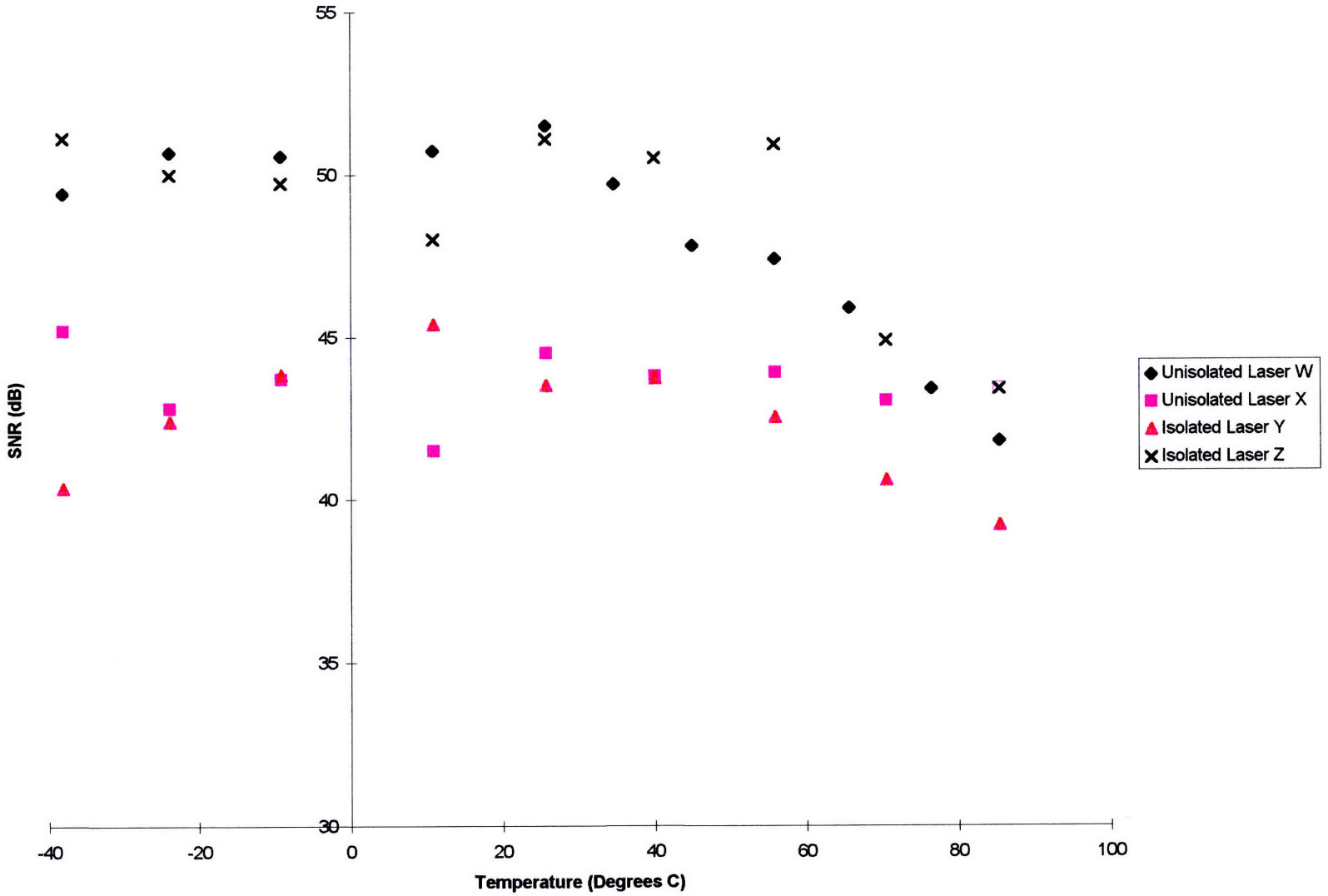

Figure 22
Signal Level vs Temperature for Isolated and Unisolated FP Lasers

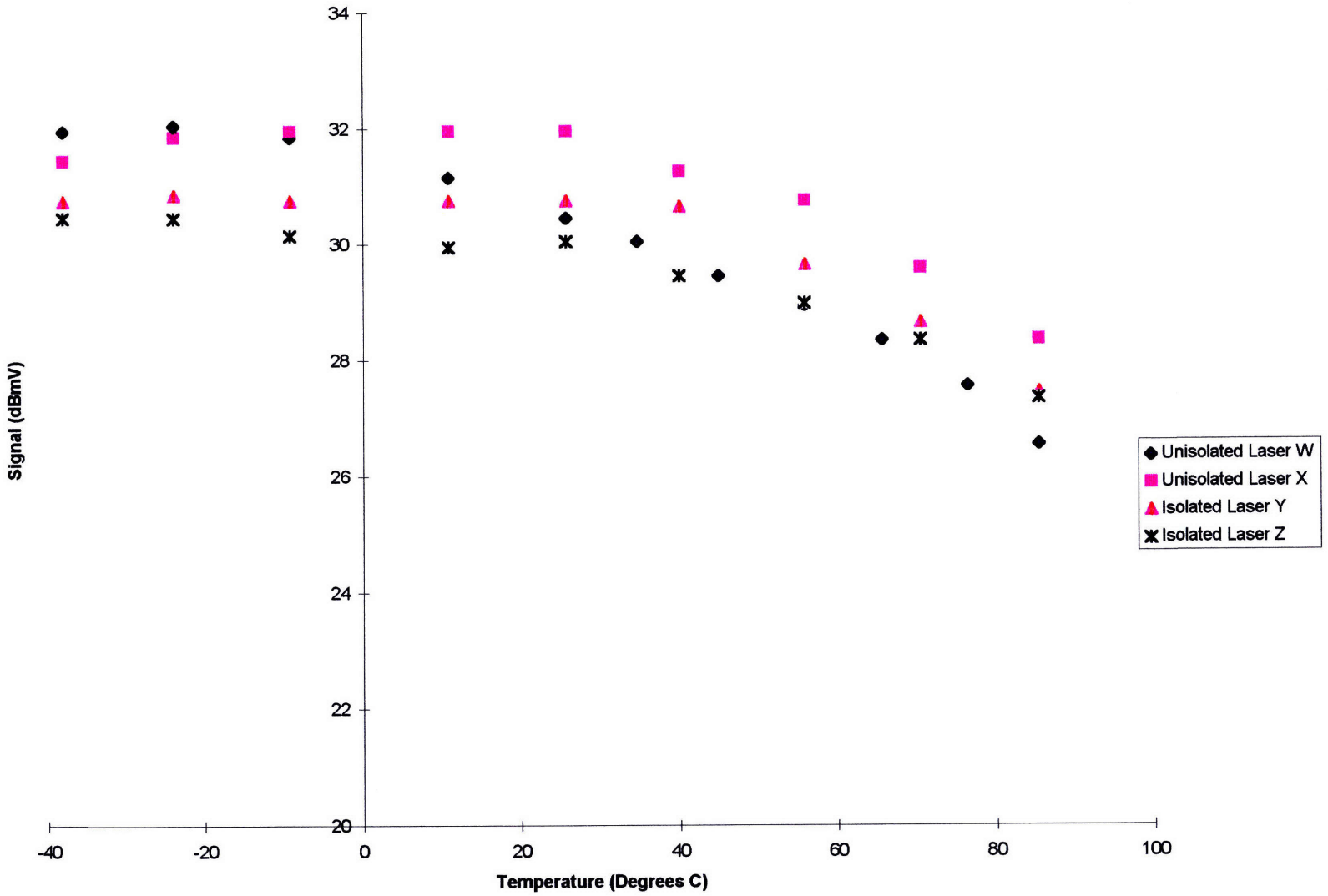

Figure 23
Noise vs Temperature for Isolated and Unisolated FP Lasers

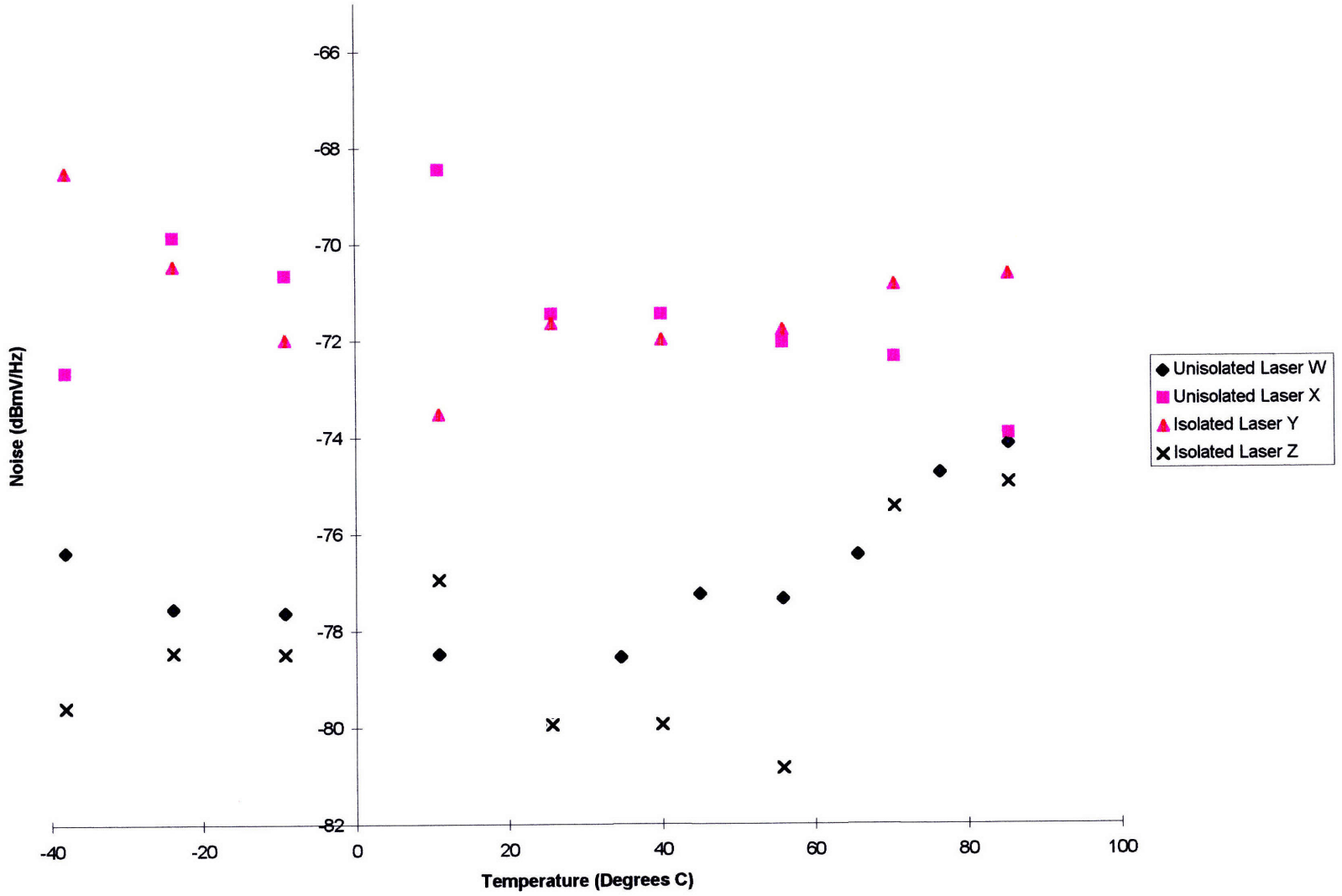

Figure 24

RIN vs Temperature for Isolated and Unisolated FP Lasers

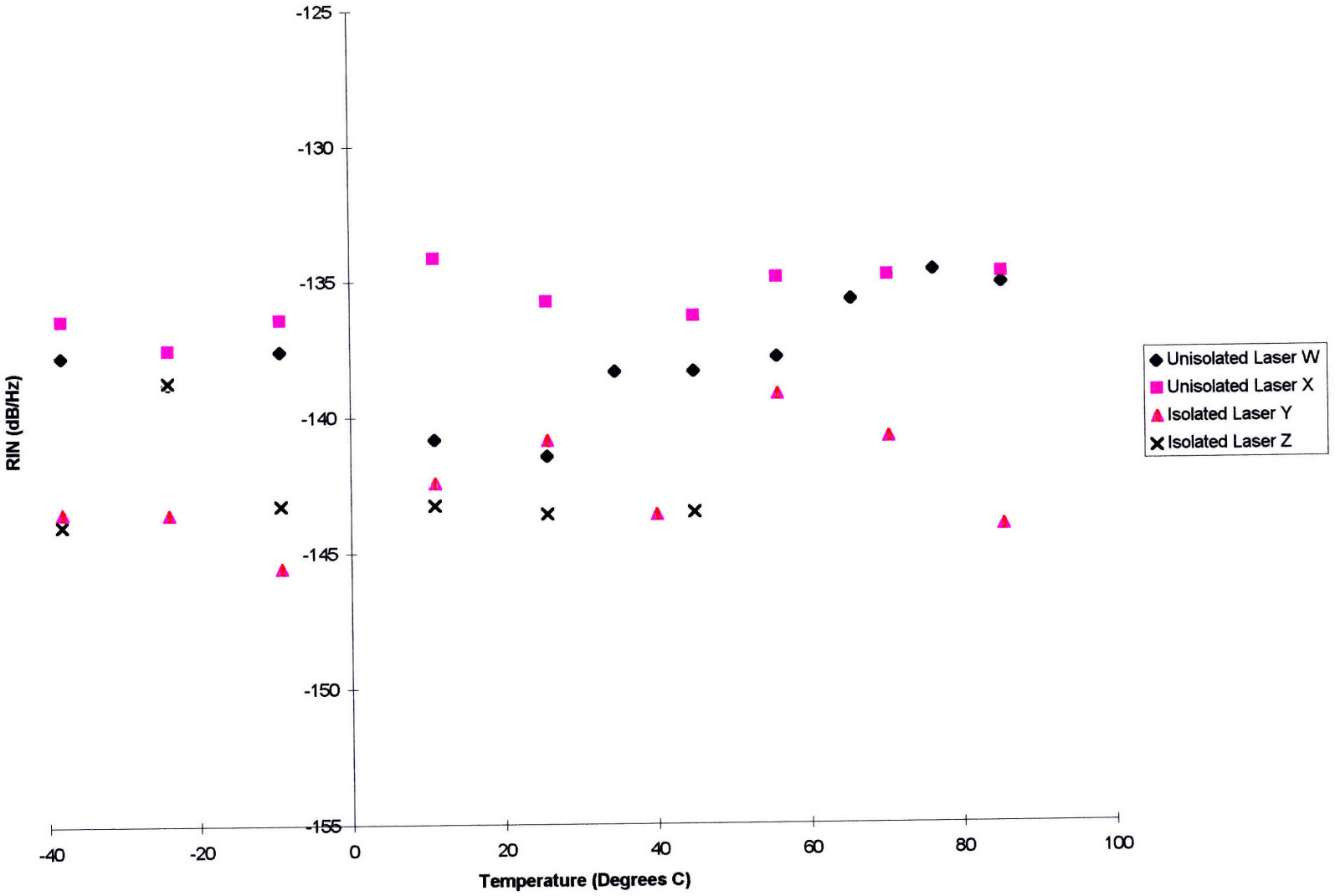

References

[1] V. Swaminathan, "A Review of Laser Technologies For Application in Hybrid Fiber-Coax Broadband Access Systems," Proceedings of High Speed III-V Electronics for Wireless Application at the 25th SOTAPOCS (Eds. F. Ren, C. S. Wu, S. N. G. Chu, and S. J. Pearton), Electrochemical Society, Pennington, N.J., 96-15, 1996, pp. 148.

[2] S.L. Woodward, G. E. Bodeep, "Uncooled Fabry-Perot Lasers for QPSK Transmission," Photonics Technology Letters, 7, 1995, pp. 558.

[3] S.L. Woodward, V. Swaminathan et. al, "Transmission of QPSK Signals Using Unisolated DFB Lasers," IEEE Photonics Technology Letters, 8, 1996, pp. 127.

[4] Denis J. G. Mestdagh, Fundamentals of Multiaccess Optical Fiber Networks, Artech House Inc., Boston 1995, pp. 31-33.

[5] Grovind P. Agrawal, Niloy K. Dutta, Semiconductor Lasers, Van Nostrand Reinhold, New York 1993, pp. 319-320.

[6] Mestdagh, pp. 36-37.

[7] G. P. Agrawal, N. K. Dutta, Long-Wavelength Semiconductor Lasers, Van Nostrand Reinhold, New York 1986, pp. 128-135.

[8] Mestdagh, pp. 186.

[9] Simon Haykin, Digital Communications, John Wiley & Sons Inc., 1988, pp. 284-290.

[10] Mestdagh, pp. 291-294.

[11] Mestdagh, pp. 102-111.

[12] Aires Alves, Lucent Technologies, MA, unpublished.

[13] Mestdagh, pp. 38-39.

[14] Mestdagh, pp. 300.

[15] T.E. Darcie, G. E. Bodeep, "Fiber-Reflection-Induced Impairments in Lightwave AM-VSB CATV Systems," Internal Memorandum, Lucent Technologies, NJ, pp. 4.

[16] Mestdagh, pp. 312-316.

[17] V. Swaminathan, Lucent Technologies, MA, unpublished.

[18] J. P. Moffat, Lucent Technologies, MA, unpublished.

[19] L. A. Campos, D. Krinsky, "Effect of Upstream Channel Distribution in the HFC Network," Hybrid Fiber-Coax Symposium, (eds.) W. S. Lai and S. T. Jewell, SPIE vol 2609, pp. 203-214 (1995).

[20] V. Swaminathan, Lucent Technologies, MA, private communication.

[21] Lawrence A. Stark, "Advantages and Performance of DFB Lasers for HFC Network Return Path Applications," Cable-Tec Expo '96 Proceedings Manual (Eds. Roberta Dainton, Raia King, Janene Martin, Howard Whitman), Society of Cable Telecommunications Engineers, Nashville, TN, 1996, pp. 124.

[22] S. B. Krasulick, A. G. Swanson, "CATV Performance of Uncooled Modules," Internal Memorandum, Lucent Technologies, SSTC, PA, 1994, pp. 2-5.